DNA damage drives antigen diversification through mosaic Variant Surface Glycoprotein (VSG) formation in *Trypanosoma brucei*

Jaclyn E. Smith[1], Kevin J. Wang[1], Erin M. Kennedy[1], Jill M.C. Hakim[1], Jaime So[1], Alexander K. Beaver[1,2], Aishwarya Magesh[1], Shane D. Gilligan-Steinberg[1,3], Jessica Zheng[1], Bailin Zhang[1,4], Dharani Narayan Moorthy[1], Elgin Henry Akin[1], Lusajo Mwakibete[1], Monica R. Mugnier[1,5*]

[1]W. Harry Feinstone Department of Molecular Microbiology and Immunology, Johns Hopkins Bloomberg School of Public Health, Baltimore, Maryland, United States of America

[2]Department of Pathology, Johns Hopkins School of Medicine, Baltimore, Maryland, United States of America

[3]Current Affiliation: Department of Bioengineering, University of Washington, Seattle, Washington, United States of America

[4]Current Affiliation: Scripps Research Department of Integrative Structural and Computational Biology, La Jolla, San Diego, California, United States of America

[5]Lead contact

*Correspondence: mmugnie1@jhu.edu (M.R.M.)

Summary

Antigenic variation, using large genomic repertoires of antigen-encoding genes, allows pathogens to evade host antibody. Many pathogens, including the African trypanosome *Trypanosoma brucei,* extend their antigenic repertoire through genomic diversification. While evidence suggests that *T. brucei* depends on the generation of new variant surface glycoprotein (VSG) genes to maintain a chronic infection, a lack of experimentally tractable tools for studying this process has obscured its underlying mechanisms. Here, we present a highly sensitive targeted sequencing approach for measuring VSG diversification. Using this method, we demonstrate that a Cas9-induced DNA double-strand break within the VSG coding sequence can induce VSG recombination with patterns identical to those observed during infection. These newly generated VSGs are antigenically distinct from parental clones and thus capable of facilitating immune evasion. Together, these results provide insight into the mechanisms of VSG diversification and an experimental framework for studying the evolution of antigen repertoires in pathogenic microbes.

Keywords:
Antigenic Variation, Variant Surface Glycoprotein, Trypanosoma brucei, Diversification, Immune evasion, DNA repair

Introduction

Pathogen survival in a host depends upon effective and continuous immune evasion. Several bacteria and eukaryotic pathogens have adopted the strategy of antigenic variation to evade host immunity, a process in which they continuously alter antigenic surface proteins to escape the host's adaptive immune response. The African trypanosome *Trypanosoma brucei*, a unicellular eukaryotic parasite and causative agent of human and animal African trypanosomiasis, uses an especially sophisticated system of antigenic variation. The parasite, which remains extracellular throughout infection and thus faces a perpetual onslaught of host antibody, periodically "switches" expression of a surface coat consisting of 10^7 copies of a single, immunogenic protein known as the Variant Surface Glycoprotein (VSG). This process allows parasites to escape host antibody and maintain a chronic infection.

Although the *T. brucei* VSG repertoire contains thousands of VSGs, this repertoire is probably too small to maintain a chronic infection through VSG switching alone. During an infection, each *T. brucei* parasite expresses a single VSG at a time from one of ~15 telomeric Bloodstream Expression Sites (the "active" BES)[1]. The remaining VSG-encoding genes are stored in other expression sites, subtelomeric arrays, and minichromosomes, all of which remain transcriptionally silenced[2]. The parasite switches its VSG either by transcriptional activation of a silent BES (*in situ* switching) or through a gene conversion event in which a new VSG is copied into the active expression site. While gene conversion-based switching allows for the activation of VSGs outside of a BES, analysis of the *T. brucei* genome has shown that only ~20% of the VSGs in the parasite genome are full-length genes encoding a functional VSG protein. The remaining ~80% of VSGs in the parasite genome consist of pseudogenes or gene fragments[2] and cannot immediately be used for immune evasion through *in situ* or gene conversion switching. Moreover, the number of VSGs expressed in a population of parasites at a single time during experimental infection sometimes exceeds the total number of intact VSGs in the parasite genome[3,4], further indicating that the repertoire of intact VSGs is insufficient to achieve the antigenic diversity required to maintain a chronic infection.

Evidence suggests that *T. brucei* deals with this shortage of antigens through diversification of the VSG repertoire. Many studies of experimental infections in mice have shown that novel VSGs, generated during infection, predominate at later stages of infection[3,5,6], while analysis of parasites from natural human infections revealed expressed VSGs that were nearly completely absent from the genomes of contemporary field isolates[7]. These observations suggest that the generation of new VSGs plays a critical role in sustaining *T. brucei* antigenic variation.

There are two mechanisms thought to be responsible for extending the VSG repertoire: mosaic formation and *de novo* point mutation. Mosaic VSGs form when two or more VSG genes combine through segmental gene conversion to form a novel VSG. This mechanism allows parasites to access pseudogenes and VSG fragments within the repertoire. While mosaic VSGs have been observed in the literature, they are often found under extreme experimental conditions[8–12] or late during infection[3,5,13,14] making it difficult

to discern how exactly they arose. VSGs also appear to occasionally acquire *de novo* point mutations, though these can be difficult to distinguish from a small gene conversion event using a similar donor VSG. The origins of these mutations also remain mysterious, though newly acquired mutations seem rare[9,15–17]. Ultimately, *de novo* mutation of VSGs would allow parasites to generate new VSG sequences regardless of the contents of their repertoire, further amplifying diversity.

Despite its clear importance, the mechanisms driving VSG diversification, whether by mutation or recombination, remain poorly understood. It is plausible that DNA damage and repair may play a role in either mechanism, as expressed VSG genes sit between two highly repetitive and damage-prone stretches of DNA, the conserved 70bp repeat and the telomere[2,18]. DNA breaks are frequently observed within the 70bp repeats at the active expression site[19,20] and near telomeres within silent BESs[20]. Experimental evidence implicates DNA damage in VSG switching more generally, as a DNA double-strand break induced upstream of the VSG induces a switch[19,20], but it is unknown whether DNA damage could also generate new VSGs.

There is a dearth of experimental evidence for the mechanisms driving VSG diversification because there has been no controlled and reproducible *in vitro* system for studying the process. Instead, researchers have had to rely on observation alone, characterizing the sequences of expressed VSGs that were isolated by chance. This approach has been crucial for generating hypotheses but is insufficient for deciphering the mechanisms driving the process. Here, we present a comprehensive toolkit for the controlled and reproducible study of the diversification of individual VSGs. Using a highly sensitive barcode-based targeted RNA-seq approach, we show that DNA double-strand breaks can trigger the formation of mosaic VSGs that are identical to those observed *in vivo* during infection. Homology appears to drive donor VSG selection, with microhomology between the parent and donor VSG flanking the site of recombination in almost every event. We demonstrate that homologous donor VSGs can be utilized as a template for DNA repair regardless of their genomic location. Finally, we observe that break-induced diversification is most efficient in the portion of the VSG gene encoding the exposed top lobe of the VSG N-terminal domain, allowing very small changes in the VSG protein to facilitate large changes in antibody binding. We suggest that this could represent a potential hypervariable region within the VSG, facilitating diversification in the region of the VSG protein where host antibody is most likely to bind.

Results

DNA double-strand breaks trigger the formation of mosaic VSGs

A number of studies have suggested that VSG diversification occurs, at least some of the time, within the active expression site[3,16], with the sequence of the actively expressed VSG being altered through recombination and/or mutation. For this reason, we focused our analyses on diversification of the actively expressed VSG. Because a double-strand DNA break upstream of the VSG within the active BES is known to induce switching[19,20], we hypothesized that a break within the VSG coding sequence might result in mosaic VSG formation. To investigate this, we engineered tetracycline-inducible Cas9 expressing EATRO1125 parasites, which express the VSG AnTat1.1, and induced breaks across the AnTat1.1 coding sequence using a set of guide RNAs.

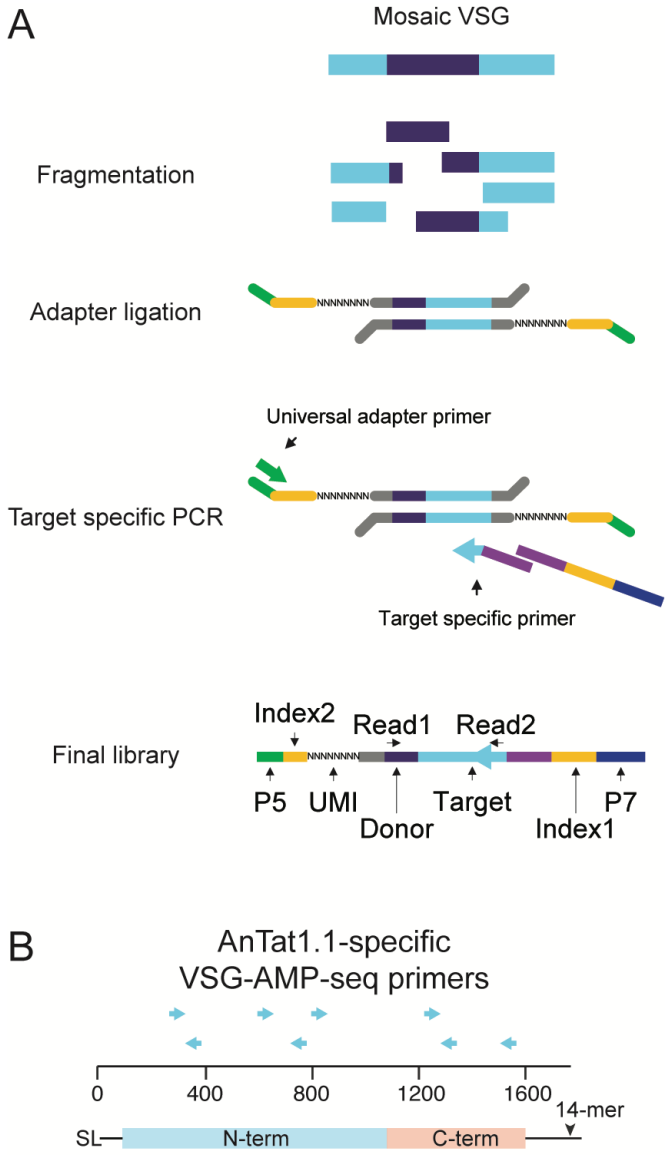

Figure 1. VSG-AMP-seq protocol
A) Schematic of the library prep for VSG-AMP-seq. Figure adapted from [65]. B) Locations of target specific primers for VSG AnTat1.1. SL = 5′ splice leader sequence, 14-mer = 3′ sequence conserved in all VSG transcripts

To evaluate potential recombination outcomes, we developed VSG Anchored Multiplex PCR Sequencing (VSG-AMP-seq), a technique that overcomes previous obstacles to studying VSG diversification by providing both high-throughput and highly accurate sequences (1A). Our approach uses long unique molecular indexes (UMIs) to generate high-confidence consensus sequences[21]. Consolidating reads into consensus sequences allows errors like PCR chimeras, which occur during later cycles of PCR and therefore represent a minority of sequences in a consensus group[22], to be eliminated while true events are retained. Libraries are prepared by fragmenting VSG-specific cDNA. Fragments are then end-repaired, A-tailed and ligated to universal adapters containing a

174 25bp UMI (1A). A VSG target of interest is selected, and a series of staggered primers
175 are designed to cover the length of the target VSG's coding sequence (1B). By pairing
176 target-specific primers with a universal reverse adapter primer, target VSG fragments are
177 amplified within a sample regardless of their identity. Mosaic reads are defined as those
178 for whom a portion of the read matches the target and the remainder matches another
179 VSG (the "donor VSG") within the VSG repertoire (VSGnome) of the strain being studied[2].
180 Due to its selective, target-specific amplification, this method can sensitively detect
181 thousands of rare diversification events, even from mixed samples where diversified
182 VSGs are a minority of the population. To validate this approach, we mixed together at a
183 known ratio two parasite clones expressing two distinct VSGs that shared sufficient
184 sequence similarity to make them prone to the generation of PCR chimeras. We then
185 performed VSG-AMP-seq on RNA extracted from this parasite mixture. This analysis
186 revealed very few erroneous recombination events, even without UMI consolidation,
187 demonstrating that VSG-AMP-seq is highly accurate and detects true mosaic
188 recombination events (Supplemental Figure 1).
189
190 To induce breaks across AnTat1.1, we induced Cas9 expression for 24 hours and
191 then transfected in DNA amplicons containing a T7 promoter and a guide RNA targeting
192 various regions throughout the AnTat1.1 coding sequence to induce breaks in the VSG.
193 Parasites were collected two days after transfection of the guide, and mosaic derivatives
194 of AnTat1.1 were analyzed by VSG-AMP-seq (2A; Supplementary Figures 2A, 2B & 3C).
195 We detected thousands of recombination events from two independently generated Cas9
196 clones (C1 = 5956, C2 = 4488).
197
198 Our analysis revealed diverse mosaic recombination events centered around each
199 break site. Such events were virtually absent from the negative (no guide) control,
200 suggesting this process does not occur at a high rate in the absence of a trigger or in the
201 presence of Cas9 alone. Notably, as the DNA breaks progressed further away from the
202 center of the AnTat1.1 coding sequence, the frequency of mosaic formation decreased
203 dramatically (2B). This did not appear to be related to the guide sequences (Supplemental
204 Figure 2C-G) or to guide cutting efficiency (Supplemental Figure 2H). To ensure that the
205 observed mosaic events represented mosaic VSGs that were truly expressed by the
206 parasite, and not technical artifacts or VSGs incapable of being stably expressed by *T.*
207 *brucei*, we also obtained individual clones of parasites expressing AnTat1.1-derived
208 mosaic VSGs. Using parasite lines that stably express a VSG-targeted guide RNA, we
209 induced Cas9 expression for 7 days (2C; Supplemental Figure 2A). We isolated 29
210 mosaic-expressing parasite clones, 4 from guide 243, 22 from guide 694, and 3 from
211 guide 1459, from a total of 5 parental cell lines. These parasites expressed VSGs
212 containing recombination events identical to those observed using VSG-AMP-seq. These
213 results suggest that DNA damage within the active VSG can trigger the formation of
214 mosaic VSGs, with recombination events centered around the site of DNA damage.
215
216 **Homology drives mosaic VSG formation**
217
218 Analysis of the mosaic recombination events detected by VSG-AMP-seq revealed
219 an important role for sequence homology in the formation of mosaic VSGs. Within the

220 isolated mosaic clones, we observed short insertions (< 200 bp, average = 49 bp, median
221 = 23 bp) predominating among the events (2D). Although read lengths limited our ability
222 to detect larger insertions with VSG-AMP-seq, approximately 55-60% of the mosaic
223 recombination reads detected by VSG-AMP-seq contained the same short insertions
224 (average C1 = 46 bp, average C2 = 45.8 bp) (Supplemental Figure 3C). Almost all (C1=
225 99.71%, C2 = 99.46%) of these recombination events occurred within a region of shared
226 sequence between AnTat1.1 and each donor VSG, with an average length of ~9 bps
227 (average C1 = 9.13 bp, average C2 = 9.44 bp, median = 6 bp) (2F; Supplemental Figure
228 1A). Notably, only a small number of donor VSGs were used for the majority of
229 recombination events. Upon closer inspection, these donors are members of a 6-VSG
230 family that contains AnTat1.1 and represent the only sequences within the EATRO1125
231 VSGnome with significant homology to this VSG (2E). N-terminal recombination events
232 appear restricted to just these family members (C1 = 100%, C2 = 99.87%). Together,
233 these results suggest that VSG sequence homology influences the outcome of VSG
234 recombination after a DNA break.
235
236 Not all VSGs share sequence homology with other members of the VSG repertoire,
237 however. To determine the outcome following DNA damage of a VSG when there are no
238 homologous donors available, we used the same Cas9 system in the commonly used
239 Lister427 *T. brucei* line to cut the actively expressed VSG, VSG-2, which lacks
240 homologous family members. After inserting stably expressed guides targeting VSG-2
241 into the genome, we induced Cas9 expression for 7 days. Parasite clones isolated after
242 a break in VSG-2 no longer expressed VSG-2, and the VSGs expressed by these clones
243 showed no evidence of mosaic recombination (Supplemental Figure 3B; cut position 707,
244 n = 4; cut position 1082, n = 3). This further supports the hypothesis that sequence
245 homology between the parent and donor VSG is required for mosaic VSG formation.
246
247 We sought to determine what proportion of the VSG repertoire contains VSGs that
248 are members of VSG families and thus capable of diversifying through break-induced
249 mosaic formation. We performed an all vs all BLAST to cluster VSGs based upon
250 sequence similarity within both the EATRO1125 and Lister427 parasite strains and found
251 that most (>75%) of the known VSG sequences are capable of diversifying through the
252 mechanisms described here (2G). We supplemented this analysis with an orthogonal
253 clustering method and estimated a similar proportion of diversifiable VSGs (Supplemental
254 Figure 3A).
255

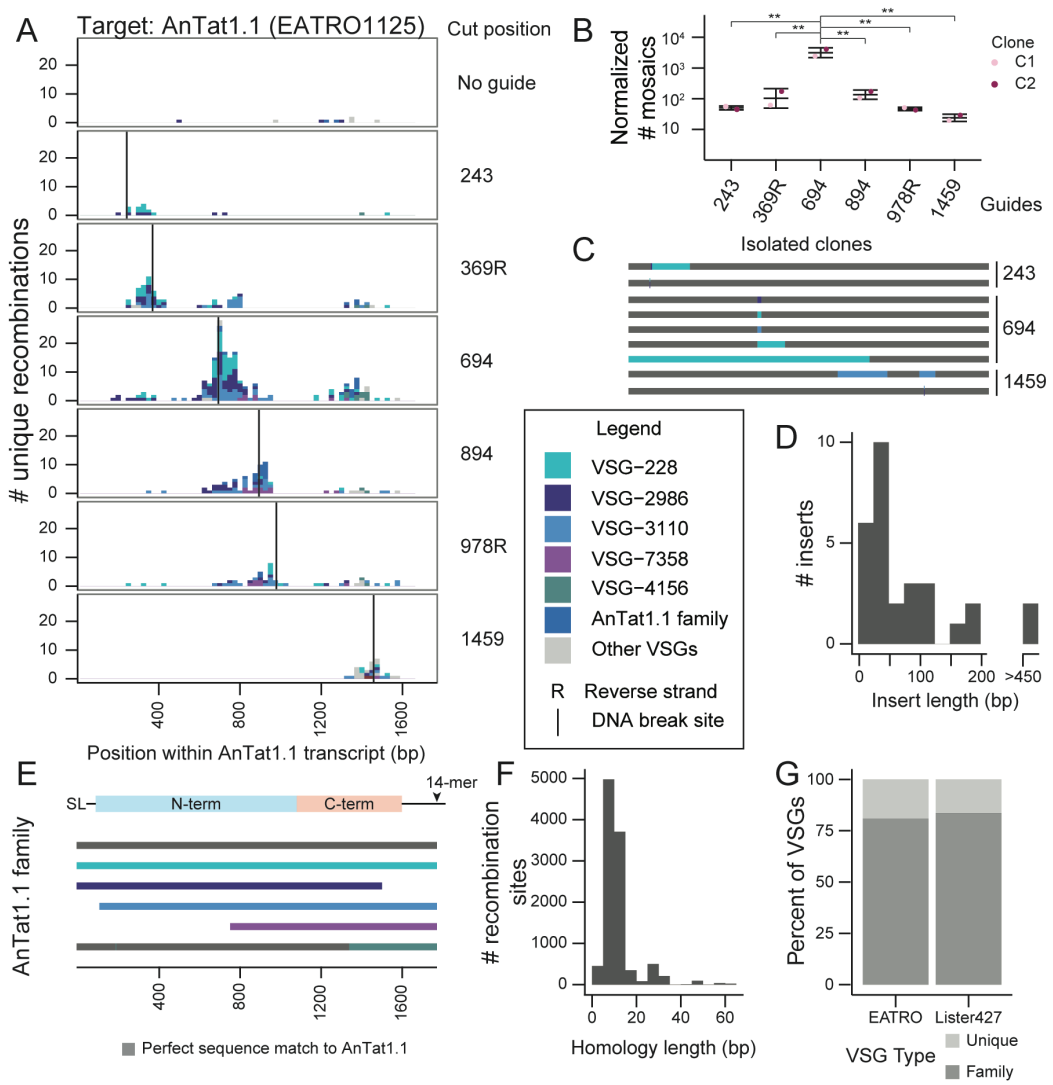

Figure 2. DNA double-strand breaks trigger mosaic VSG formation when homology is available
A) A histogram of unique recombination events identified along the AnTat1.1 transcript. The Cas9 DNA break site is indicated by a vertical line. Cut positions, relative to the 5' end of the VSG transcript are: 243, 369, 694, 894, 978, and 1459. Sections of the histogram are colored to indicate donor VSG identified. R indicates a guide that binds to the reverse strand. The midpoint of the perfect homology between AnTat1.1 and the donor VSG at the recombination site is plotted. If a mosaic sequence matched >1 potential donor VSG, the average recombination position was plotted. B) Quantification of mosaic recombination events induced by DNA breaks. The number of recombination events detected within 250bp up or downstream of the cut site was normalized to the number of total unanchored reads aligning within that region compared to the unanchored read count from the region with the smallest coverage to control for sequencing depth. (n=2, two independent clones) Statistical significance was determined with a one-way ANOVA with post-hoc Tukey HSD (** p <0.01) Mean ± s.d. C) Schematics of mosaic VSGs from parasite clones isolated after DNA breaks within AnTat1.1. Representative sequences shown. D) A histogram of donor VSG insertion lengths identified in all isolated mosaic-expressing clones. The insert length only includes newly inserted sequence and does not include recombination sites. E) A schematic of the AnTat1.1 family aligned to the AnTat1.1 transcript. Gray sequences are a perfect match to AnTat1.1. F) A histogram of the length of the shared identity between AnTat1.1 and the donor VSG at each recombination site. G) Quantification of types of VSGs within the VSGnomes from EATRO1125 and Lister427 parasites. The Lister427 VSGnome has 5 VSGs which are perfectly duplicated without any other family members. SL = 5′ splice leader sequence, 14-mer = 3′ sequence conserved in all VSG transcripts

257 **Donor VSGs act as templates for break-induced VSG diversification**
258
259 Although most AnTat1.1-derived mosaics were identical to the putative donor VSG, many
260 of these insertions altered only a few bps in AnTat1.1. We thus reasoned that it was
261 possible that these events were *de novo* mutations created during DNA repair that
262 happened to match the putative genome-encoded donor VSG. To test this possibility, we
263 took advantage of the unique VSG repertoires in the EATRO1125 and Lister427 parasite
264 strains[2,23]. While AnTat1.1 is not endogenously present in Lister427 parasites, there are
265 five VSGs nearly identical to the AnTat1.1 family member VSG-2986 (99.5%, 98%,
266 97.5%, 95.5%, and 92.2% nucleotide sequence identity) (3A, Supplemental Figure 4).
267 These VSGs, if mosaic recombination were templated, could serve as donor VSGs for
268 the formation of AnTat1.1-derived mosaic VSGs. We thus engineered dox-inducible
269 Cas9-expressing Lister427 parasites and replaced VSG-2 with AnTat1.1 at the active
270 expression site, BES1. We then induced breaks in AnTat1.1 as before and detected
271 hundreds of recombination events in two independent clones (L1-A1 1 = 398, L1-A2 =
272 833; 3C). All mosaic recombination events detected utilized donor VSGs found
273 exclusively in the Lister427 genome (3B), indicating that the repair events that generate
274 mosaic VSGs require a template.
275

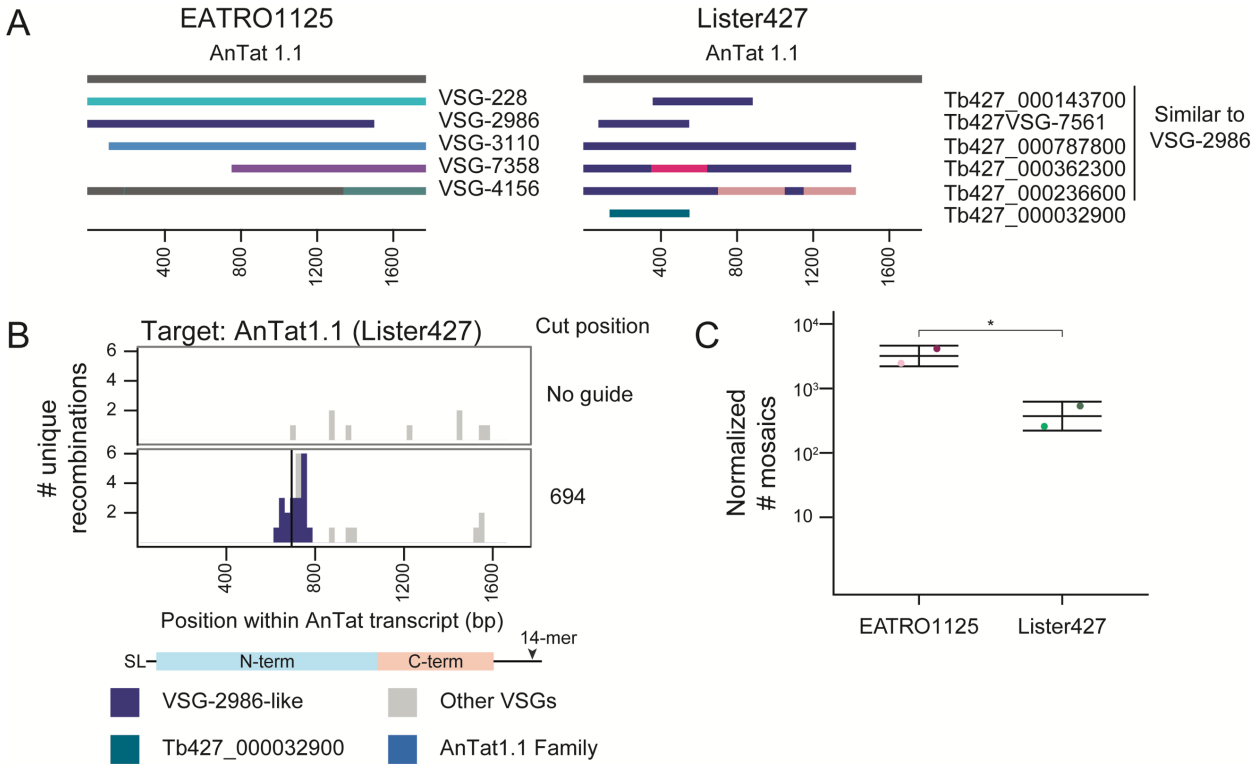

Figure 3. Nucleotide changes observed in mosaic VSGs arise from templated insertions
A) Schematics of the EATRO1125 AnTat1.1 VSG family and the VSGs similar to AnTat1.1 found within Lister427. Each is aligned to the AnTat1.1 transcript. For regions that are identical between two donor VSGs, regions are shown in the same color. B) A histogram of unique recombination events identified within AnTat1.1-expressing Lister427 parasites after a cut at position 694 along the AnTat1.1 transcript. The midpoint of the perfect homology between AnTat1.1 and the donor VSG at the recombination site is plotted. All AnTat1.1 family members except VSG-2986 were included as potential identifiable donor VSGs (all Lister427 VSGs + VSG-228, VSG-3110, VSG-7358, and VSG-4156). C) Quantification of mosaic recombination events induced by Cas9 at position 694. EATRO data is from 2A and 2B. The number of recombination events detected within 250bp up or downstream of the cut site was normalized to the number of total unanchored reads aligning within that region compared to the unanchored read count from the region with the smallest coverage from the EATRO cut sites to control for sequencing depth. Mean ± s.d. SL = 5′ splice leader sequence, 14-mer = 3′ sequence conserved in all VSG transcripts

276
277

Donor VSGs can be utilized for mosaic recombination even within non-VSG loci

We wondered whether the location of a VSG within the genome could influence its utilization as a donor for mosaic recombination. To evaluate the role genomic context plays in the selection of donor VSGs, we again took advantage of the unique repertoires of the EATRO1125 and Lister427 strains[2], as well as the high quality, phased genome assembly of the Lister427 parasite strain[23]. Using the same AnTat1.1-expressing Lister427 Cas9 parasites, we inserted an EATRO1125 VSG, VSG-228, which is commonly used as a donor in AnTat1.1 mosaics and is absent from Lister427 parasites, into three genomic locations: the minichromosomes, where VSGs are typically found, and the rDNA spacer and the tubulin array, where VSGs are not typically stored (Supplemental Figure 4). We then induced breaks at position 694 in AnTat1.1 and analyzed donor selection by VSG-AMP-seq (Figure 4).

The endogenous Lister427 donors were selected at the same frequency in all samples, suggesting that the presence of an additional donor did not interrupt the formation of these mosaic VSGs. Surprisingly, the inserted donor, VSG-228, was utilized regardless of its location. Notably, only the coding sequence of VSG-228 was inserted into the Lister427 background. This indicates that neither the upstream 70-bp repeats typically found interspersed within the VSG archive[24–27] or the 5'- and 3'-UTRs of the VSG are required for locating donor templates. Taken together, these data suggest that parasites possess a sophisticated homology search mechanism that allows donor VSGs to be utilized regardless of genomic location.

301

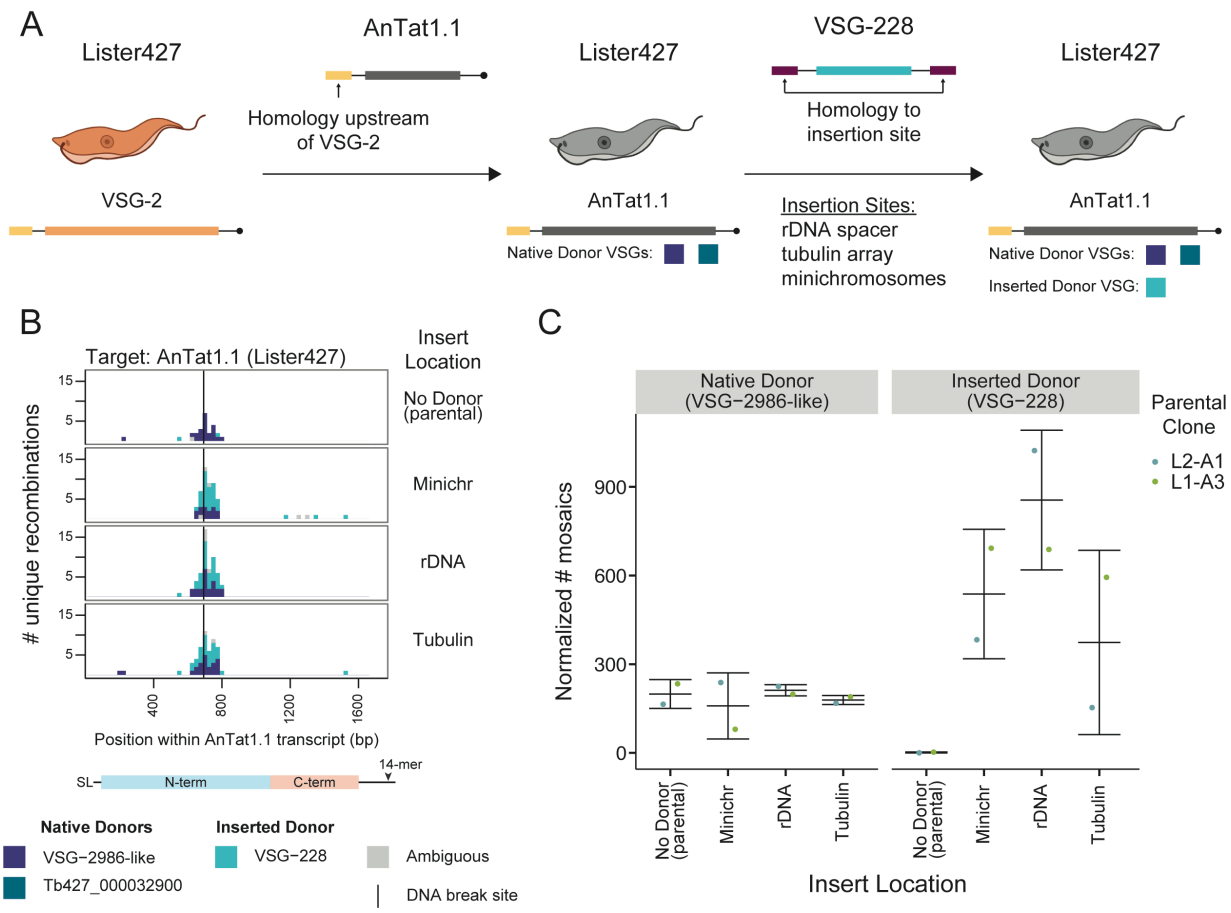

Figure 4. Donor VSGs are accessible throughout the genome

A) A schematic of the generation of Lister427 parasites expressing AnTat1.1 and harboring a silent copy of VSG-228. Available donor VSGs for the actively expressed VSG in each cell line are depicted below the parasites. B) A histogram of unique recombination events after a cut at position 694 in AnTat1.1 in Lister427 parasites expressing AnTat1.1 with VSG-228 inserted into the genome. The midpoint of the perfect homology between AnTat1.1 and the donor VSG at the recombination site is plotted. EATRO1125 AnTat1.1 family members were tested as potential identifiable donor VSGs (VSG-2986, VSG-228, VSG-3110, VSG-7358, and VSG-4156). C) Quantification of mosaic recombination utilizing VSG-2986-like or VSG-228 as a donor sequence at position 694 following induction of Cas9. The number of recombination events detected within 250bp up or downstream of the cut site was normalized to the number of total unanchored reads aligning within that region compared to the unanchored read count from the region with the smallest coverage. Each parental clone was independently generated. Mean ± s.d. SL = 5′ splice leader, 14-mer = 3′ sequence conserved in all VSG transcripts *T. brucei* cartoons created with Biorender.com

302 **Mosaic VSGs generated *in vitro* are identical to a subset of mosaic VSGs formed *in***
303 ***vivo***
304
305 To investigate whether the mosaic VSGs we detected after break induction *in vitro*
306 reflected the events that occur naturally *in vivo*, we performed VSG-AMP-seq on parasites
307 isolated from wildtype mouse infections, on day 15 post-infection, when AnTat1.1 has
308 been mostly eliminated from the blood (Supplemental Figure 5B & 5C). We observed a
309 strong C-terminal bias to all recombination events (316 recombination events across 7
310 mice). Very few sequences aligned to AnTat1.1 within the N-terminus, suggesting that
311 most of these mosaic VSGs were complete replacements of the VSG N-terminal domain
312 (5A; Supplemental 5A). These donor VSGs shared significantly less homology with
313 AnTat1.1 than the AnTat1.1 family members, usually only sharing spans of 100bps or
314 less of imperfect homology within the C-terminal region of the VSGs. Nevertheless, there
315 was still a short (average = 12 bp) span of perfect identity between AnTat1.1 and the
316 donor at the recombination site (5E). Since VSGs expressed by parasites at the second
317 peak of parasitemia are antigenically distinct from AnTat1.1, we reasoned these N-
318 terminal replacement VSGs ensured complete immune evasion since only a small portion
319 of AnTat1.1 was retained.
320
321 We wondered whether the restriction of events to the VSG C-terminus reflected a
322 mechanistic bias towards recombination within the VSG C-terminal domain or the effect
323 of host antibody selection, with only the most immune evasive recombination events
324 surviving. To investigate these possibilities, we repeated the experiment in μMT mice[28],
325 which do not have B-cells and therefore do not generate antibodies. We again analyzed
326 day 15 post-infection, though AnTat1.1 is never cleared from these infections and
327 parasitemia remains high throughout (Supplemental 5B & 5C). In μMT mice, mosaic
328 recombination events span the full length of the VSG, and many are identical to mosaic
329 VSGs observed *in vitro* (5A; Supplemental Figure 5A) (2144 recombination events across
330 7 mice). *In vivo,* we observe short insertions (average = 41 bp) using donors homologous
331 to AnTat1.1 flanked by short (average = 13 bp, median = 9 bp) regions of perfect identity,
332 matching the patterns we observed *in vitro* (5E & 5F). Interestingly, as in the wildtype
333 infections, there are an additional subset of recombination events within the C-terminus
334 which are largely absent *in vitro* and use a much more diverse set of donors (5B). These
335 data demonstrate that our *in vitro* system recapitulates a subset of *in vivo* recombination
336 events, but there may be other pathways facilitating recombination *in vivo* in addition to
337 those that can be triggered by a single, blunt DNA double-strand break.
338
339 **Mosaic VSGs form in extravascular spaces during infection**
340
341 While AnTat1.1 is eliminated from the blood in wildtype mice, it persists within
342 tissues until at least day 14[4]. Given that parasite clearance is delayed in extravascular
343 spaces, we wondered if mosaic formation may occur more readily in this parasite niche.
344 To investigate this, we analyzed all assembled VSGs from a previous study of
345 extravascular parasite populations[4]. Again, we found AnTat1.1 mosaics present in tissues
346 identical to those observed in both μMT mice and *in vitro* (5C & 5G). Moreover, we
347 observe that mosaic derivates of AnTat1.1 increase over time within tissue spaces during

infection (5D). Together, these data suggest that mosaic VSGs form preferentially within extravascular spaces, possibly due to the slower VSG-specific parasite clearance in these spaces.

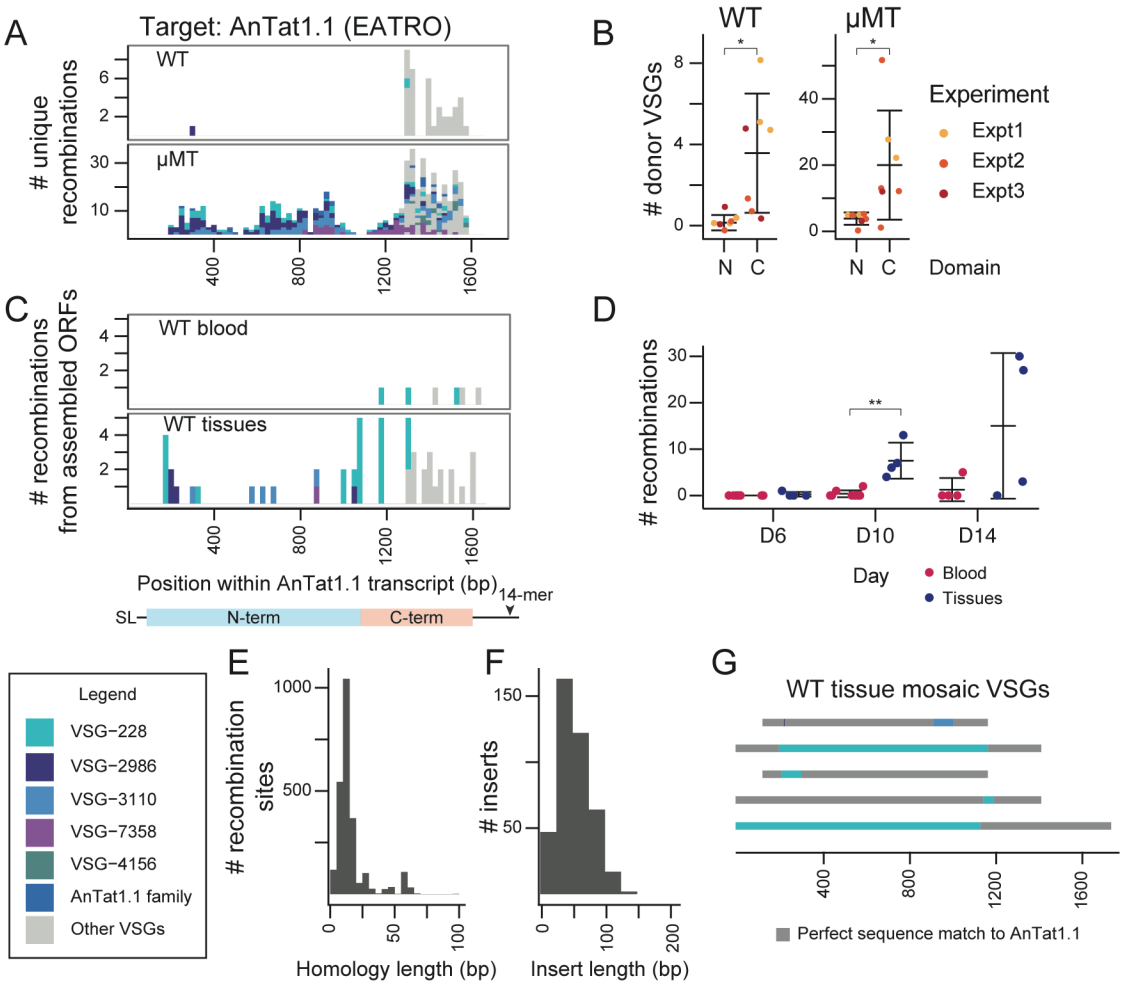

Figure 5. AnTat1.1 mosaic VSGs form *in vivo* and are most prevalent in extravascular spaces
A) A histogram of unique recombination events identified in all mice in wildtype or μMT mice from Day 15 post-infection. Recombination events found in multiple mice are represented once. (WT n=7; μMT n=7, from 3 independent experiments) The midpoint of the perfect homology between AnTat1.1 and the donor VSG at the recombination site is plotted. If a mosaic sequence matched >1 potential donor VSG, the average recombination position was plotted. B) Quantification of the number of donor VSGs utilized in mosaic recombination events within the N and C terminal domain of AnTat1.1 in wildtype and μMT mice from A). Statistical significance determined by a pairwise Wilcoxon test (*p<0.05) Mean ± s.d. C) A histogram of the mosaic recombination events identified from VSG ORFs assembled in Beaver et al.[4] All recombination events identified are shown at all time points sampled during infection: D6, D10, and D14. If a mosaic recombination event was identified in more than one tissue within the same mouse, it was counted once (n=12, 4 mice per tissue time point). D) Quantification of the mosaic recombination events detected within wildtype mouse blood or tissue. Statistical significance determined by pairwise Wilcoxon within each timepoint. (**p<0.01) Mean ± s.d. E) A histogram of the length of the shared identity between AnTat1.1 and the donor VSG at the recombination sites. F) A histogram of donor VSG insertion lengths identified within individual reads. The insert length only includes newly inserted sequence and does not include recombination sites. G) Representative schematics of mosaic VSGs from assembled ORFs in Beaver et al.[4] SL = 5′ splice leader sequence, 14-mer = 3′ sequence conserved in all VSG transcripts

351 **Small changes in the VSG sequence provide substantial antibody evasion**
352
353 Many AnTat1.1-derived mosaic VSGs differ from their original sequence by only a
354 few amino acids. To determine how these changes impacted the antigenic character of
355 the mosaic VSGs, we analyzed live parasites expressing AnTat1.1 mosaic derivatives by
356 flow cytometry using a potent rabbit anti-AnTat1.1 polyclonal antibody raised against
357 purified AnTat1.1 protein[29] (6A). Many of the mutations block about 50% of antibody
358 binding. Interestingly, three VSG-2986 mosaic clones were isolated with increasing
359 insertion length (6B). The smallest insertion (Mosaic 2: 18bps, resulting in 3 a.a.
360 changes), appears to account for most of the antigenic change, with only small decreases
361 in binding associated with each additional length of insertion. We modeled the structure
362 of these mosaics using ColabFold[30] and their general structures matched AnTat1.1 (6C),
363 except at the disordered top of the N-terminal lobe. A careful examination of the locations
364 of the mutations on AnTat1.1 show that mutations from Mosaic 2 which have the largest
365 effect on antibody binding are at the apex of the structure while other alterations can be
366 found on the side of the monomer (6D). These results demonstrate that, although the
367 insertions characteristic of mosaic recombination are quite short, even these small
368 changes to the VSG can confer large consequences for host antibody binding depending
369 on their position.
370

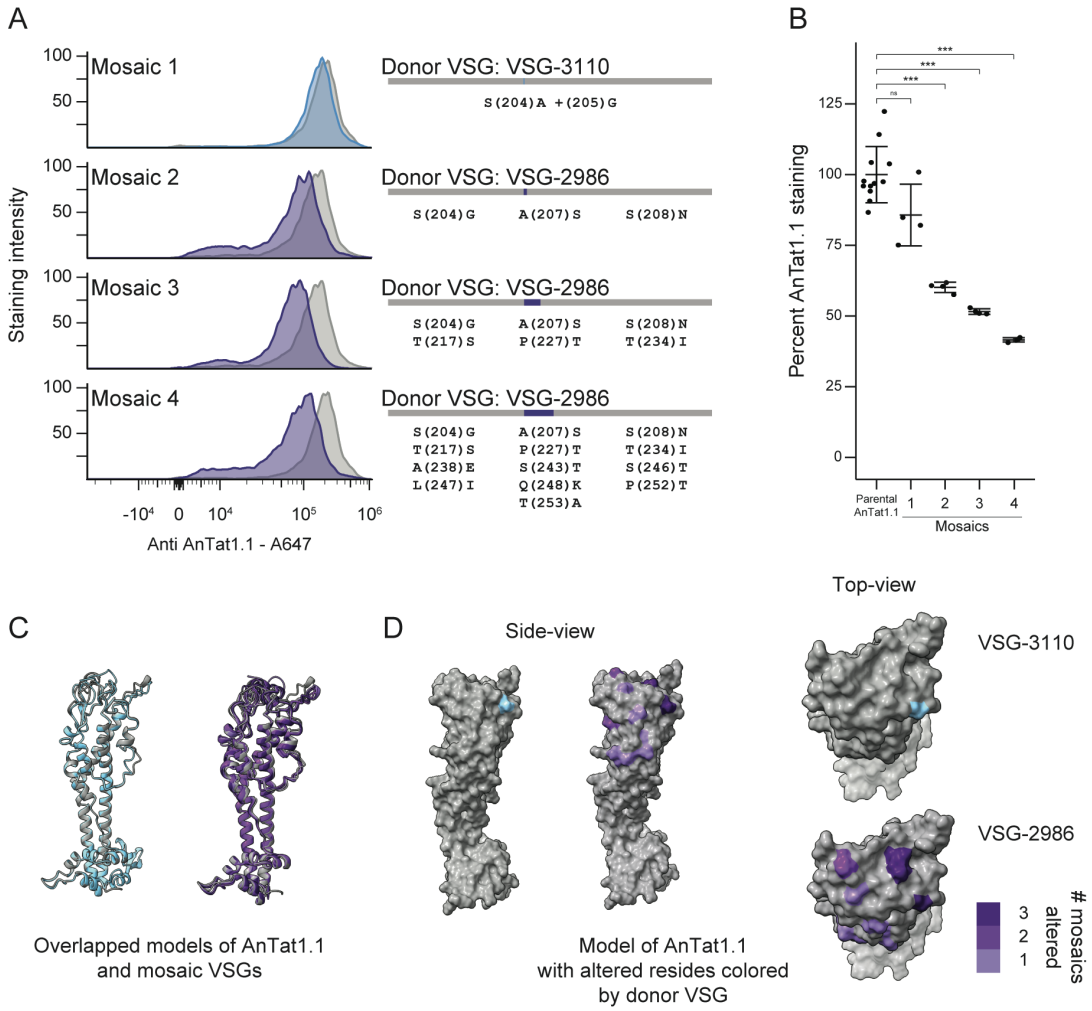

Figure 6. Mutations in sequences encoding the top of the VSG alter antibody binding
A) A histogram showing the binding of anti-AnTat1.1 antibody, as measured by anti-rabbit IgG Alexa Fluor 647 staining intensity, for parental controls (gray) and mosaic clones colored by donor VSG. (n= 4, from 3 independent parental lineages derived from 2 Cas9 clones) Schematics showing the mosaic VSGs are to the right. Donor VSG and amino acid substitutions are specified. B) Quantification of staining intensity changes for individual clones, based on median staining intensity. The median Alexa Fluor 647 intensities were normalized to the average of the parental clone. Statistical significance was determined based on a one-way ANOVA with a post-hoc Tukey HSD. (***p<0.001) Mean ± s.d. C) Overlapping ribbon structures of AnTat1.1 and Mosaic 1 in blue and AnTat1.1 and Mosaic 2, Mosaic 3, and Mosaic 4 in purple as predicted by ColabFold. D) A space filling model of AnTat1.1 highlighting the changed residues within the monomer. VSG-3110 in blue and VSG-2986 in purple.

371

Discussion

Chronic *T. brucei* infection relies on the generation of new VSGs, with novel VSGs dominating late stages of infection[3,5,6]. However, the new VSGs generated during infection are complex, possibly arising from several intermediate events, and selected within a host environment with immunity against numerous previously expressed VSGs. The inherent complexity of chronic infection thus obscures the underlying biological principles driving VSG diversification. Here, we demonstrate that VSG diversification can be induced *in vitro* using Cas9-mediated double-strand DNA breaks within the VSG coding sequence, reproducibly generating mosaic VSGs that faithfully recapitulate mosaics formed naturally *in vivo*. By selecting just one VSG and looking at thousands of recombination outcomes, we have defined patterns characteristic of mosaic recombination. Mosaic VSGs typically form through short, templated insertions, and homology drives this process, restricting donor VSGs within the N-terminus to those from a set of closely related family members. Finally, we demonstrate that mosaic VSGs provide substantial immune evasion, particularly when these changes occur at the top of the VSG N-terminus, which may reflect a hypervariable region within the VSG.

We have shown that DNA breaks, previously shown to drive VSG switching[19,20], can also result in VSG diversification through mosaic VSG formation. While the exact DNA repair mechanism that generates mosaics is unclear, the patterns we observe—short templated insertions that rely on short stretches of sequence homology—suggest this is not the canonical homologous recombination that mediates many VSG switch events. Homologous recombination relies on RAD51, an enzyme which binds free DNA ends at double strand breaks and stabilizes insertion into an intact DNA duplex, ultimately facilitating recombination. RAD51-dependent reactions in *T. brucei* require stretches of perfect homology of ~100 bp[31], and mismatches within the homology dramatically ablate recombination[31]. No recombination events detected here fit these restrictions; the maximum shared homology without a mismatch is 58 bp. In line with this, there is evidence for a RAD51-independent pathway capable of driving antigenic variation in *T. brucei*[32]. A set of *in vitro* studies in *T. brucei*[31,33] suggested that the RAD51-independent recombination mechanism utilizes shorter homology sequences[31,33] and more effectively tolerates mismatches between the target and donor sequences[31]. These patterns are more consistent with the recombination events we observe here, suggesting that mosaic formation may be driven by a RAD51-independent mechanism. While DNA repair utilizing short homology has been described in *T. brucei*[33–38], the molecular details of the mechanism remain unknown. It will be critical to follow up on this study, given the tools we have now developed, to determine the precise mechanisms driving mosaic formation.

One surprising aspect of mosaic formation is the remarkably sensitive homology search mechanism capable of locating just 1600 bp of donor VSG sequence from genomic locations where VSGs are not typically stored. This was particularly unexpected given the structured organization of the VSG repertoire, with silent VSG genes primarily restricted to the subtelomeres[24–27] and minichromosomes[39,40] among interspersed fragments of 70 bp repeats. These conserved repeats have been thought to be critical mediators of the majority of VSG switch events by acting as upstream homology to VSGs

418 within the silent subtelomeric and minichromosomal repertoires[41]. Ultimately, removing
419 70 bp repeat elements did not interrupt the homology search mechanism used for mosaic
420 formation, suggesting the repeats are not required to identify a mosaic VSG donor
421 template. This further reinforces our hypothesis that the repair mechanism driving mosaic
422 formation is distinct from that driving VSG switching. With a search mechanism so
423 sensitive, we suspect even small, extremely degenerate VSG fragments may be used by
424 the parasite for DNA repair, resurrecting ancient VSG sequences for use in novel antigen
425 formation.
426
427 While our data suggest most VSGs in the archive are capable of diversification
428 through the mechanism we have described, this is not the case for all VSGs. Indeed, we
429 find that mosaic recombination occurs only if a homologous donor VSG is available. Most
430 studies of antigenic variation in *T. brucei* have focused on VSG-2, a unique VSG that
431 does not readily diversify; this may explain, at least in part, why mosaic recombination
432 has been observed so rarely *in vitro* until now. The proportion of VSGs within families is
433 surprisingly high in both the EATRO1125 and Lister427 strains. Perhaps the VSG
434 repertoire has evolved to provide a balance between diversification events, which allow
435 significant expansion of the antigenic repertoire but may not always provide full immune
436 evasion, and switching, which is more likely to completely escape pre-existing immunity.
437
438 While the members of the AnTat1.1 VSG family provide numerous possibilities for
439 recombination and the generation of new VSGs, we found that the center portion of the
440 gene appears to be especially successful at generating recombinants. We considered
441 that this might be attributable to available donor sequences or guide efficiency, but there
442 was nothing apparently unique about this site compared to other break locations. Protein
443 modeling of AnTat1.1, however, revealed that this region encodes the top of the N-
444 terminal lobe of the VSG, a site directly exposed to host antibody. For AnTat1.1 and many
445 similar VSGs[2] (A2-type), this is an unstructured region[42], and indeed the apex of most
446 crystalized VSGs appears unstructured despite a surprising variety of underlying
447 structures[42]. We propose that this disordered region may have evolved to be more
448 tolerant to amino acid changes, allowing diversification within the part of the protein most
449 likely to facilitate immune evasion. While many recombination events may occur after a
450 DNA break, we hypothesize that only a few, particularly those within disordered regions,
451 maintain VSG structural integrity. Since expression of the VSG is essential for cell cycle
452 progression[43], it is possible that many newly formed mosaic VSGs lead to cell death for
453 the parasites, allowing only a subset of the recombination events to survive and resulting
454 in an apparent increase in recombination within the regions of the VSG where mutation
455 is most tolerated.
456
457 Indeed, even very small changes within the top of the VSG N-terminal lobe can
458 confer substantial immune evasion. Just three amino acid substitutions, from an 18 bp
459 templated replacement, block approximately 50% antibody binding from a potent
460 polyclonal antiserum. However, a 50% drop in binding may not be sufficient to fully evade
461 preexisting anti-VSG antibody. Perhaps as a result, mosaic VSGs derived from AnTat1.1
462 in WT blood appear to be mostly N-terminal replacements where the AnTat1.1 N-terminal
463 domain is completely replaced. A wider diversity of AnTat1.1-derived mosaics can be

464 observed within the tissues, however, where AnTat1.1-expressing parasites linger due to
465 differences in immune pressure[4]. In μMT mice, where AnTat1.1 expressing parasites can
466 linger indefinitely, this effect is further amplified. We thus hypothesize that generating new
467 VSGs is an iterative process, where a series of recombination events progressively shifts
468 the character of a VSG until an immunologically distinct variant is formed. The relatively
469 "protected" tissue spaces may serve as a site for this iterative process to occur. Another
470 intriguing possibility is that partial immune evasion is advantageous for the parasite: a
471 recent study suggested that exposure to sublethal antibody concentrations can trigger a
472 VSG switch in *T. brucei*[44]. Perhaps parasites expressing these partially evasive variants
473 are more prone to switching to a completely new VSG.
474
475 In addition to shedding light on the selective pressures imposed upon mosaic
476 variants, our mouse data also demonstrate that our *in vitro* model of antigenic
477 diversification recapitulates VSG diversification *in vivo*. The recombination events we
478 detect in μMT mice represent the full breadth of possible recombination events which
479 AnTat1.1 can form, and these are largely represented within our *in vitro* break-induced
480 mosaic VSG populations. We observe short insertions flanked by short regions of identity
481 in both contexts, but the dominance of the 694 break position we observe *in vitro* is not
482 reflected in our *in vivo* analysis. This could be for a variety of reasons, including non-
483 uniform break locations along the VSG *in vivo* or a variety of DNA break types driving a
484 different pattern of outcomes. Intriguingly, in the absence of an exogenous DNA break,
485 we do not observe any diversification *in vitro*, while diversification occurs continuously in
486 the μMT context. This suggests that some aspect of the host environment other than
487 antibody pressure induces diversification *in vivo.* It remains to be investigated whether an
488 *in vivo* cue for diversification exists.
489
490 The diversification mechanisms we have described, where homology templated
491 DNA repair drives antigen evolution, may also be at play in other gene families where
492 diversity is critical. Many pathogens rely on diverse antigen genes to escape the host
493 immune system, expressing one variable antigen from a silent repertoire stored within
494 subtelomeric regions of the genome, which are inherently susceptible to DNA damage.
495 Moreover, many eukaryotic pathogens that utilize antigenic variation (e.g. *Plasmodium*,
496 *Giardia*, and *Trypanosoma*) have lost canonical non-homologous end-joining DNA
497 repair[45], suggesting an important role for alternative RAD51-independent repair
498 mechanisms. Importantly, mosaic antigens have been observed in *Plasmodium*
499 *falciparum* var genes[46–49] and giardia variant-specific surface proteins (VSPs)[50,51], some
500 of which resemble the small insertion mosaics we have described here. Notably, the large
501 subtelomeric multigene family of PIR genes in plasmodium[52,53], which may drive antigenic
502 variation in both *Plasmodium vivax* malaria and rodent malarias, lacks the repeat
503 elements associated with most subtelomeric antigens[54], a feature that is not required for
504 this mechanism of DNA repair. Given these observations, we suspect the pathway
505 described here may contribute to the evolution of antigen repertoires in many diverse
506 organisms. Further, many alternative forms of DNA repair are also conserved in
507 mammals[55]; it is thus plausible that large gene families like olfactory receptors[56,57] and
508 protocadherins[56], which depend upon diversity and are known to swap sequences
509 through gene conversion events[58–61], may also be diversifying through similar

510 mechanisms. A rigorous targeted approach, like we have used here, may be required to
511 determine the role this mechanism plays in the diversification of other gene families.
512
513 Here we answer long-standing questions about how the *T. brucei* VSG repertoire
514 evolved to generate new antigens critical for maintaining a chronic infection. Our high-
515 throughput, sensitive technique has enabled the characterization of thousands of mosaic
516 diversification events, orders of magnitude more than was previously feasible. This
517 analysis revealed a pattern of short, homology-driven, and templated insertions around
518 DNA break sites that can shift the antigenic character of the VSG. More broadly, this study
519 provides an experimental framework for the hypothesis-driven exploration of antigen
520 diversification, not only in *T. brucei* but also in other pathogenic microbes.
521

522 **Methods**
523
524 **Lead contact:**
525 Further information and requests for resources and reagents should be directed to
526 and will be fulfilled by the lead contact, Monica Mugnier (mmugnie1@jhu.edu).
527
528 **Materials availability:**
529 Plasmids associated with this study will be deposited to Addgene.
530
531 **Data and code availability:**
532 Raw sequencing reads from VSG-AMP-seq and VSG-seq was deposited to the
533 NCBI Sequence Read Archive under project: PRJNA1140873
534 FASTQ files from assembled VSGs expressed by isolated parasite clones can be
535 found at github.com/mugnierlab/Smith2024
536 Original code associated with this study can be found at
537 github.com/mugnierlab/Smith2024
538
539 **Parasites:**
540 Pleiomorphic EATRO1125 AnTat1.1 90-13 *T. brucei* parasites were maintained in
541 HMI-9 media with 10% heat inactivated FBS and 10% Serum Plus. Parasites were
542 passaged when they reached approximately $5*10^5$ cells/mL. Monomorphic Single Marker
543 Lister427 VSG221 TetR T7RNAP bloodstream form (NR42011; LOT: 61775530)[62]. *T.*
544 *brucei* were maintained in HMI-9 up to $1*10^6$ parasites/mL. VSG221 has since been
545 renamed to VSG-2.
546
547 **Plasmids:**
548 Plasmids were synthesized with Gibson Assembly. Gibson Assembly master mix
549 was custom made[63]. Whole plasmid sequencing was performed by Plasmidsaurus using
550 Oxford Nanopore Technology and their custom analysis and annotation pipelines.
551
552 pLEW100v5-BSD-FLAG-La-Cas9 was synthesized from pLEW100v5-BSD and
553 pRPaCas9[64]. A *T. brucei* codon optimized FLAG tag was added to the N-terminus of
554 Cas9. pLEW100V5-BSD was a gift from George Cross (Addgene plasmid #27658;
555 http://n2t.net/addgene:27658; RRID:Addgene_27658). pRPaCa9 was a gift from David
556 Horn (Addgene plasmid #111819; http://n2t.net/addgene:111819;
557 RRID:Addgene_111819).
558
559 pHH-HYG-AnTat1.1 and pHH-HYG-VSG-228 were synthesized from pHH-HYG-
560 VSG-3-S317A.[65] This was a gift from Joey Verdi. AnTat1.1 sequence was obtained from
561 AnTat1.1 specific cDNA from mouse infection D6 cloned into a pMiniT vector with the
562 PCR Cloning Kit (NEB, E1202S). VSG-228 was partially amplified from VSG PCR (see
563 below) derived from AnTat1.1 depleted D16 μMT parasites from blood. The partial
564 fragment was amplified with an AnTat1.1 family specific forward primer (5' -
565 ACTACACCCACAACAAGCTCTA-3') and a pan VSG reverse primer which binds to a
566 conserved 14bp region of the 3' UTR (5'-
567 GATTTAGGTGACACTATAGTGTTAAAATATATC-3') with AmpliTaq Gold (Applied

568 Biosystems, 4398881) (anneal & extension 60C 1m, 35 cycles).The resulting PCR was
569 cloned into the pMiniT backbone and the remainder of VSG-228 was *de novo* synthesized
570 with Gibson Assembly.
571
572 The pT7sgRNA plasmids were obtained according to Rico et al.[64] Briefly, sticky-
573 end annealed sgRNAs were ligated into a BbsI-HF (NEB, R0539S) digestion of
574 pT7sgRNA. Table 1 contains the sequences for the annealed guides. pT7sgRNA was a
575 gift from David Horn. (Addgene plasmid #111820; http://n2t.net/addgene:111820;
576 RRID:Addgene_111820)
577
578 pHD309-PUR-VSG-228 was synthesized from pHD309-HYG-PUR. To obtain a
579 plasmid for VSG-228 insertion, the sequence encoding the puromycin resistance gene
580 was replaced with VSG-228. To convert the plasmid from hygromycin resistance to
581 puromycin resistance, the sequence encoding the hygromycin resistance gene was
582 replaced by the puromycin resistance gene. pHD309-HYG-PUR was a gift from George
583 Cross. (Addgene plasmid #24014; http://n2t.net/addgene:24014; RRID:Addgene_24014)
584
585 pLEW100v5-PUR-VSG-228 was synthesized from pLEW100v5-BSD. The
586 sequence encoding the blasticidin resistance gene was replaced with puromycin
587 resistance. The sequence encoding the firefly luciferase was replaced with VSG-228. The
588 rRNA promoter and the Tet operator sequences upstream of VSG-228 were removed.
589
590 pLEW100v5-PURO-177-VSG-228 was synthesized from pLEW100v5-177-HYG.
591 The sequence encoding the hygromycin resistance gene was replaced with puromycin
592 resistance. The sequence encoding firefly luciferase was replaced with VSG-228. The
593 Tet operator sequences were removed. pLEW100v5-177-HYG was a gift from George
594 Cross. (Addgene plasmid # 24013; http://n2t.net/addgene24013; RRID:Addgene_24013)
595
596 pLEW100v5-PURO-T7-sgRNA was synthesized from pLEW100v5-PUR-VSG-228
597 and pT7sgRNA. 5' UTRs for Fructose 1,6-bisphosphate aldolase replaced the Actin 5'
598 UTR for puromycin expression. Actin and GPEET 5'UTRs were removed as they have
599 BbsI restriction sites within them. A T7 promoter was added to drive PURO expression.
600 The T7-sgRNA cassette from pT7sgRNA was inserted into the modified pLEW backbone.
601 Target specific constructs were obtained as above for pT7-sgRNA.
602
603 **Transgenic parasites:**
604 To obtain all transgenic parasites, 5 million parasites were electroporated with 5-
605 10ug of digested plasmid with an AMAXA Nucleofector II using X-001 in Human T-cell
606 Nucleofector Solution (Lonza VPA-1002).
607
608 For tetracycline-inducible Cas9 parasites, EATRO1125 or Lister427 parasites
609 were electroporated with pLEW100v5-BSD-FLAG-La-Cas9, digested with NotI-HF (NEB,
610 R3189S). Parasites were immediately selected in 5ug/mL blasticidin (Thermo Scientific,
611 R21001) and maintained in selection unless otherwise specified.
612
613 To obtain AnTat1.1 and VSG-228 expressing Lister427 parasites, Lister427

614 parasites were electroporated with pHH-HYG-VSG plasmids digested with BamHI-HF
615 (NEB, R3136S). After 16-24 hours recovery, 25ug/mL of hygromycin (Fisher Scientific,
616 J67371-XF) was added to the culture. After obtaining colonies 5-7 days later, selection
617 was reduced to 5ug/mL and maintained unless otherwise specified.
618
619 Lister427 parasites with pLEW100v5-BSD-FLAG-La-Cas9 inserted were
620 additionally electroporated with pHH-HYG-VSG plasmids expressing Antat1.1. Clones
621 were obtained as above.
622
623 To obtain AnTat1.1 Lister427 parasites with silent VSG-228 donors inserted, these
624 parasites were additionally electroporated with pHD309-PUR-VSG-228, pLEW100v5-
625 PURO-VSG-228 or pLEW100v5-PURO-177-VSG-228 plasmids digested with NotI-HF.
626 After 16-24 hours of recovery, 0.1ug/mL of puromycin (Millipore Sigma, P8833) was
627 added to the culture. Parasites were maintained in puromycin, and 5ug/mL of blasticidin
628 and hygromycin unless otherwise specified.
629
630 To obtain constitutive guide expressing parasite lines, inducible Cas9-expressing
631 parasites (both Lister427 and EATRO1125 Cas9 strains) were electroporated with
632 pT7sgRNA guide containing plasmids digested with NotI-HF[64]. After 16-24 hours
633 recovery, single colonies of parasites were selected with 2ug/mL phleomycin (Sigma-
634 Aldrich, SML3001). Parasites were maintained without phleomycin selection. These
635 parasites were used to obtain parasite clones following DNA break induction.
636
637 To obtain constitutive guide expressing parasite lines with puromycin selection
638 rather than phleomycin, EATRO1125 inducible Cas9-expressing parasites were
639 electroporated with pLEW-T7-sgRNA digested with NotI-HF. After 16-24 hours of
640 recovery single colonies were selected with 0.1ug/mL of puromycin. Cultures were
641 maintained in 0.1ug/mL puromycin and 5ug/mL blasticidin unless otherwise specified.
642 These parasites were used for western blot analysis and to obtain parasite clones
643 following DNA break induction.
644
645 **T7-Guide synthesis & purification:**
646 DNA fragments containing a T7 promoter and guide RNA sequence were
647 synthesized as described previously[66]. Briefly, T7-guide primers and a G00 primer were
648 amplified with Phusion polymerase for 35 cycles (annealing temp 60C, extension 5s).
649 PCR products from 12 identical PCRs were pooled and purified via ethanol precipitation.
650
651 **Cas9 transient electroporations:**
652 Approximately 24 hours prior to electroporation, parasites were seeded at a
653 density of 83,000 parasites/ml and induced with 1ug/mL doxycycline (Millipore Sigma,
654 D9891-1G). The total culture volume of was determined by the number of samples being
655 electroporated; 12mLs were seeded per sample. Blasticidin selection (Cas9) and
656 puromycin selection (silent VSG-228) were maintained, if applicable, and for Lister427
657 parasites expressing AnTat1.1, hygromycin (active VSG expression) was removed at this
658 stage. Either 8mLs (Lister427) or 10mLs (EATRO1125) of the bulk parasite culture,
659 approximately 5-10 million cells, were spun down for each sample. Media was then

660 removed, and parasites were resuspended in 100uL Human T-cell Nucleofector Solution.
661 Each sample was electroporated using the X-001 program on the AMAXA Nucleofector
662 II with approximately 1-1.5ug of purified T7-guide in a volume less than 10uL or a sample
663 without any DNA as a negative control. Parasites were moved into 5mLs HMI-9 in 6-well
664 plates to recover for 30 minutes then moved into 20mLs total in flasks to recover
665 overnight. About 24 hours after electroporation, parasites were counted and split. For
666 EATRO1125, 12 million cells (or all cells if there were fewer than 12million) were seeded
667 into 60mLs total with blasticidin. For Lister427, 2 million cells were seeded into 20mLs
668 total with blasticidin. At the 48 hour time point, parasites were counted, collected, and
669 stored in TRIzol (Invitrogen, 15596026) for subsequent RNA extraction.
670
671 **Isolation of mosaic expressing parasites:**
672 Multiple parasite clones expressing T7sgRNA with guides at cut sites 243 and 694
673 were derived from two distinct inducible Cas9-expressing parasite clones with constitutive
674 guide expression driven by pT7-sgRNA. Multiple dilutions of parasites were plated in 96-
675 well plates in 5ug/mL blasticidin and 1ug/mL doxycycline. Parasite clones were isolated
676 from plates containing fewer than 30 individual surviving parasite clones. Most plates
677 contained fewer than 10. Individual clones were visible after 7-14 days. Upon isolation of
678 a parasite clone, all drugs were removed. A subset of parasites were analyzed by flow
679 cytometry.
680
681 A single parasite clone expressing pLEW-T7-sgRNA with a guide at position 1459
682 was derived from an inducible Cas9-expressing parasite clone. Multiple dilutions of
683 parasites were plated in 96-well plates in 5ug/mL blasticidin, 0.1ug/mL puromycin, and
684 1ug/mL doxycycline. Parasites were isolated from plates containing fewer than 30
685 surviving parasite clones. Individual clones were visible after 7-14 days. Upon isolation of
686 a parasite clone, all drugs were removed.
687
688 VSG sequences for clones were determined from extracted RNA. cDNA was
689 synthesized using the Superscript III Reverse Transcriptase (Invitrogen, 18080051) and
690 a VSG-specific primer which binds to a conserved 14-bp sequence within the 3' UTR. (5'-
691 GTGTTAAAATATATC-3'). 2uL of RNase-treated cDNA was amplified for 35 cycles with
692 VSG specific primers: a spliced-leader (5'-ACAGTTTCTGTACTATATTG-3') and SP6-
693 VSG 14-mer (5'-GATTTAGGTGACACTATAGTGTTAAAATATATC-3') using Phusion
694 polymerase (Thermo Fisher, F530L) (annealing temp 55C, extension 45s). PCR products
695 were cleaned using the Monarch PCR & DNA cleanup kit (NEB, T1030L). VSG
696 sequences were determined by amplicon nanopore sequencing performed by
697 Plasmidsaurus using Oxford Nanopore Technology with their custom analysis and
698 annotation where fragmented VSG amplicons were sequenced and assembled into full
699 length sequences or targeted Sanger sequencing with the sequencing primer (5'-
700 AGAGAATACTAAGCTAGTTGGC-3') performed by Azenta Life Sciences.
701
702 **Mouse infections:**
703 All experiments involving mice were performed in accordance with the protocol
704 approved by the Institutional Animal Care and Use Committee at Johns Hopkins
705 University. 8-12 week old female C57BL/6 mice and μMT^{-} (B6.129S2-Ighm^{tm1Cgn}/J)[28] mice

706 (Jackson Labs) were infected with ~5 EATRO1125 parasites by intravenous injection in
707 the tail vein. These parasites express either AnTat1.1 or VSG-421. Starting at D4 post-
708 infection, parasitemia was monitored within mice every two days via tail bleed. Blood was
709 harvested at D6 post-infection through a submandibular bleed. An additional gel pack and
710 in-cage food pellets were provided to mice during recovery. At D15 post-infection, mice
711 blood was harvested by cardiac puncture. Blood was stored in TRIzol LS (Invitrogen,
712 10296028) for RNA extraction.
713
714 **RNA preparation:**
715 Parasites were stored in TRIzol prior to RNA extraction. Blood with parasites was
716 stored in TRIzol LS. RNA was extracted via phenol/chloroform extraction according to the
717 manufacturers protocol. Purified RNA was DNase treated with Turbo DNase (Thermo
718 Fisher, AM2239) and purified with 1.8X Mag-Bind TotalPure NGS Beads (Omega Bio-
719 tek, M1378-01). Verification of effective DNase treatment was performed via PCR of
720 hygromycin (EATRO1125 only) (Fwd: 5'-ACAGCGGTCATTGACTGGAG-3'; Rev: 5'-
721 ATTTGTGTACGCCCGACAGT-3', annealing temp 52C, extension 30s) or HSP70
722 (Lister427 & EATRO1125) (Fwd: 5'-AGAACACTATCAATGACCCCAAC-3'; Rev: 5'-
723 CCATGCCCTGGTACATCT-3', annealing temp 50C, extension 15s) genes for 30 cycles
724 using OneTaq DNA Polymerase (NEB, M0480L).
725
726 **VSG-seq:**
727 VSG-seq was performed as previously described[3,4]. Briefly, cDNA was
728 synthesized using the Superscript III Reverse Transcriptase and a VSG-specific primer
729 which binds to a conserved 14-bp sequence within the 3' UTR. (5'-GTGTTAAAATATATC-
730 3'). cDNA was treated with Rnase A (Qiagen, 19101) and RNase H (Invitrogen,
731 18080051) for 30 minutes then purified with 1.8X Mag-Bind Total NGS Beads (Omega
732 Bio-tek, M1378-01). Purified cDNA was amplified for 25 cycles with VSG specific primers:
733 a spliced-leader (5'-ACAGTTTCTGTACTATATTG-3') and SP6-VSG 14-mer (5'-
734 GATTTAGGTGACACTATAGTGTTAAAATATATC-3') using Phusion polymerase
735 (Thermo Scientific, F530L) (annealing temp 55C, extension 45s). This PCR product was
736 prepared for sequencing following a 0.6X bead clean up using the Nextera XT DNA
737 Sample Prep Kit (Illumina, FC-131-1096) according to the manufacturer's instructions.
738 Libraries were sequenced with 100 bp single-end reads on a NovaSeq6000. Analysis was
739 performed using the VSGSeqPipeline found at github.com/mugnierlab.
740
741 **VSG-AMP-seq library preparation:**
742 VSG-AMP-seq was based upon AMP-seq[67] and GUIDE-seq[68]. cDNA was
743 synthesized from DNA-free RNA using Superscript III Reverse Transcriptase and a VSG-
744 specific primer which binds to a conserved 14-bp sequence within the 3' UTR. (5'-
745 GTGTTAAAATATATC-3'). Second Strand synthesis was performed with NEBNext
746 mRNA Second Strand Synthesis Module (E6111L). The resulting double stranded cDNA
747 was purified with 1.8X Mag-Bind Total NGS Beads. cDNA was fragmented briefly with
748 NEBNext dsDNA Fragmentase (M0348L) for ten minutes at 37C to obtain fragments of
749 approximately 500bps. Fragments were purified with a double-sided Mag-bind bead
750 cleanup. First, fragments were incubated with 0.5X beads, DNA bound to the beads were
751 discarded and an equal volume of beads as before, then a 1X PEG concentration, was

752 added to the fragments and the cleanup proceeded as normal. Fragments were end-
753 repaired with Enzymatics low concentration end repair mix (Y9140-LC-L) and A-tailed
754 with Recombinant Taq (Life Technologies, 100021276). Y-Adapters were pre-annealed
755 by incubating a MiSeq Common Adapter with Adapters (A01-A10) containing 25 bp
756 Unique Molecular Indexes (UMIs) and a barcode at 10uM at 95C for 1 sec, 60C for 1s,
757 and slowly cooled to 4C. Adapters were ligated to the A-tailed fragments with T4 DNA
758 Ligase (Enzymatics L6030-LC-L). The resulting fragments were cleaned up with 0.8X
759 Mag-Bind beads. Two target specific PCRs were performed on the fragments with pools
760 of target specific primers, one in the forward and one in the reverse direction. All primers
761 are listed in Table 1. Target primers have spacers of varying lengths to generate
762 sequence diversity without the need for PhiX. Target specific primers are paired with P5_2
763 and a sample specific P primer (P701-P710) which contains a second barcode.
764 Fragments are amplified with Platinum Taq (Life Technologies, 10966018) using the
765 following program: 95C 5 mins, 35 cycles of 95C for 30s, 55C for 30s, and 72C for 30s,
766 and 72 for 5 mins. The resulting products were cleaned up with 0.6X Mag-bind beads.
767 Libraries were quantified using the Qubit dsDNA HS Kit (Life Technologies, Q32854) and
768 run on a 1% agarose gel to determine average length. Libraries were sequenced on a
769 MiSeq or for deep sequencing of μMT samples on a NovaSeq6000 with custom index1
770 and read2 primers using the following cycle conditions: "151|8|33|131" with the paired-
771 end Nextera sequencing protocol.
772
773 **VSG-AMP-seq analysis:**
774 Index sequences were added to the names of sequencing reads. FASTQ files were
775 demultiplexed by target specific primer using cutadapt v=3.5[1] searching for multiple
776 target-specific primers at the 5' end of read2 in paired-end mode using flags --
777 action=retain --overlap 10. Then, reads were quality trimmed with trim_galore v0.6.4_dev
778 (github.com/FelixKrueger/TrimGalore) where adapter sequences, if present, were
779 removed with flags --dont_gzip --paired --trim1. Spacers were removed from read1 if
780 present using cutadapt by searching for the target-specific primer sequence at the 3' end
781 of the read with flags --action=retain --overlap 10. Dual-indexed barcodes were used to
782 demultiplex reads. A custom function in the pipeline (barcode_errors()) was used to the
783 identify number of mismatches permitted so all barcodes present could be unambiguously
784 identified.
785
786 To consolidate reads, UMIs were extracted from large FASTQ files, split into
787 smaller files and grouped by 100% identity using cd-hit-est v4.8.1[70,71] with flags -c 1.0 -n
788 8 -M 16000 -d 0. UMIs were then grouped by 92% (no more than 2 mismatches per UMI)
789 using flags -c 0.92 -n 8 -M 16000 -d 0. Reads were sorted into consensus groups based
790 on UMIs and a consensus sequence was formed as the most popular base at each
791 position of the read with a threshold quality score of at least 2. If there was a tie, an N
792 was used. Clusters with fewer than 3 reads were removed. Consolidation was only used
793 for samples isolated from mouse infections.
794
795 The full sequence of the AnTat1.1 transcript was determined by Plasmidsaurus
796 using Oxford Nanopore Technology with their custom analysis and annotation. However,
797 in our initial analyses of control samples, we determined that many reads slightly differed

near the splice leader, suggesting that transcripts might be alternatively spliced or included extra sequence appended at some point during the library preparation process, specifically adjacent to splice leader. We defined the AnTat1.1 reference as the full-length variant determined by Plasmidsaurus sequencing, with the longest splice variant observed in control samples (no guide, electroporated) appended to the 5'-end. When reads did not align to this reference, they were then compared against the ten most commonly observed AnTat1.1 isoforms to account for all possible variations in the AnTat1.1 transcript. These sequences, including the full length AnTat1.1 reference, can be found in global_target.py. The positions were 0 indexed. Read2, the anchored read, was aligned to AnTat1.1. Read pairs were removed if: the first 4/10 bases after the primer did not align to AnTat1.1, an alternative VSG which contained the primer sequence was amplified, the wrong position of AnTat1.1 was amplified by the anchor, if the reads were too short (<15 bps), contained too many Ns (>5), if there was an inversion event or a duplication, or if the transcript was alternatively spliced. Read1, the unanchored read, was also aligned to AnTat1.1 with a mismatch of up to 1bp. If no alignment could be found, read1 was trimmed to remove AnTat1.1 like sequences from the 5' and 3' ends, allowing up to 1 mismatch on each end to be removed, leaving a fragment which can be used to search the VSGnome and identify potential donor VSGs. A consensus sequence was generated from the reads, if they overlapped, using their alignment positions within AnTa1.1. AnTat1.1, the consensus read, and putative donor VSG were aligned, and recombination sites were identified. If no consensus could be generated from the two reads, read1 was used. Ambiguous recombination sites where the mosaic portion of a read matched more than one donor were represented by the average position of the potential recombination sites and identified as ambiguous. Mosaic reads which did not overlap to generate a consensus and did not contain an identifiable recombination site in read1 were excluded from analysis.

Identification of mosaic VSG from ORFs in Beaver et al.[4]

ORFs from Beaver et al.[4] were tiled into 20 bp k-mers overlapping by 1bp each. All tiles were aligned to AnTat1.1 using bowtie[72] with the following flags: -v 2. ORFs where 15 or more tiles successfully aligned to the AnTat1.1 sequence were identified as possible mosaics (≥ 35 bp match, potentially discontinuous). AnTat1.1 sequence containing ORFs were assessed for sequence matching common donor VSGs: VSG-228, VSG-2986, VSG-3110, and VSG-7358. If a best match could not be determined or if recombination did not occur with one of the typical donor VSGs, VSG sequences were analyzed by hand to identify remaining mosaic recombination events.

VSG clustering and family identification:

VSGs were identified from annotated genes and pseudogenes from the TriTrypDB-66 Lister427 2018 genome GFF[23]. Those identified with an attribute including "VSG" or "variant" but not "invariant", "Invariant", "histone", "Histone", "RING", "ubiquitin", "exclusion", "Exclusion", "nonvariant", or "Nonvariant". Many known VSGs were only annotated as an unknown protein product. To identify additional VSG-encoding genes, we isolated all unknown gene products with attributes including "hypothetical protein", "pseudogene" or "unknown", but not including "VSG", "variant" or any of the additionally excluded words above. VSGs were identified among these unknown genes via BLAST

844 against all known VSG-encoding sequences (Those from Cross et al.[2], the EATRO1125
845 VSGs with flanking sequences from George Cross, Beaver et al.[4], and TriTrypDB-66[73]
846 TRU927, Lister427, and EATRO1125 genomes.) Genes were considered a VSG if the
847 blast hit extended over 80% of the unknown gene and had a bitscore of 500 or greater.
848 We identified an additional 2545 VSGs.
849
850 All Lister427 identified VSGs from the Lister427 2018 genome and the FASTAS
851 from Cross et al.[2] (vsgs_tb427_all_atleast150aas_cds.txt,
852 vsgs_tb427_nodups_atleast250aas_cds.txt,
853 vsgs_tb427_nodups_atleast250aas_cdsplusflanks.txt) were combined and duplicate
854 VSGs were removed with cd-hit-est with the following flags: -c 1.0 -n 8 -M 16000 -d 0.
855 VSGs with identical sequences, but distinct positions within the 2018 genome were added
856 back for a total of 8564 VSGs. In the Lister427 2018 genome, we identified 5789 VSG-
857 encoding genes total and included 300bps flanking sequences up and downstream of the
858 coding sequence for further analysis. These are genes visualized in Supplemental Figure
859 4.
860
861 EATRO1125 VSGs were obtained from TrypsRU (George Cross) and included 200
862 bp flanking sequences. (vsgs_tb1125_all_atleast150aas_cdsplusflanks.txt) Duplicate
863 genes were removed with cd-hit-est with the following flags: -c 1.0 -n 8 -M 16000 -d 0.
864
865 To define VSG families, network analysis was performed using the curated VSG
866 reference FASTA files described above. Each genomic repertoire was subjected to an
867 all-versus-all BLASTn run under the default parameters to generate pairwise tables which
868 contained the query-subject pair, query sequence length, alignment length, E-value and
869 percent identity. Networks were generated with the igraph R package[74,75] using
870 undirected and unweighted clustering of nodes after applying link cutoffs based on E-
871 value < 1e-20 and alignment coverage of the query sequence > 80%. The leading
872 eigenvector clustering method (function: cluster_leading_eigen()) was used to detect
873 communities and assign nodes based on their connectivity.
874
875 To supplement the BLAST network graph approach, the greedy clustering
876 UCLUST algorithm[76] was used to assess clusters of VSGs. VSGs were clustered using
877 usearch with the following flags: -id .75 -strand both -sizeout -sort length -maxhits 2. For
878 each genome, identified VSGs were sorted by sequence length then clustered at a global
879 identity threshold of 75%
880
881 **Western blotting:**
882 EATRO1125 parasites with pLEW-FLAG-La-Cas9 and pLEW-T7sgRNA were
883 grown for 24 hours in the presence of doxycycline or DMSO vehicle control. Post
884 induction, 5 million parasites were harvested and washed with 25C PBS. Then, pelleted
885 parasites were resuspended in 50uL RIPA buffer (50mM Tris, 150mM NaCl, 1% NP-40,
886 0.5% Sodium Deoxycholate, 0.1% SDS, pH = 7.4) + 2X Laemmli buffer. Lysed parasites
887 were boiled at 95C for 5 minutes. 5uL of lysates were separated on a Tris-glycine
888 polyacrylamide gel at 110V for 100 minutes in Tris/glycine running buffer (25mM Tris,
889 192mM glycine, 0.1% SDS, pH = 8.3). Proteins were then transferred onto a nitrocellulose

890 membrane using transfer buffer (25mM Tris, 192mM glycine, 20% methanol) overnight at
891 a 60mAmps per transfer box at 25C. For Cas9 (1:1000) and EF1α (1:1000), lysates were
892 separated on 10% polyacrylamide gels and transferred onto 0.45µm membranes. For γ-
893 H2A (1:200), lysates were separated on a 15% polyacrylamide gel and transferred onto
894 a 0.2µm membrane. After transfer, blots were blocked with 0.5% BSA in TBS with 0.05%
895 Triton X-100 (TBST, 20mM Tris, 150mM NaCl, pH = 7.6) for an hour at RT under constant
896 agitation. Blots were incubated with primary antibody (see above dilutions) for 2 hours at
897 25C. After 5 TBST washes, blots were stained for 1 hour with goat anti mouse (1:5000,
898 Cell Signaling, 7076S) or goat anti rabbit-HRP-conjugated secondary (1:5000, Cell
899 Signaling, 7074S). After another 5 washes, blots were incubated with ECL (Cytiva,
900 RPN2109) and film was exposed to blots in a dark room. Developed film was scanned
901 and images were processed with FIJI[77]. Primary antibodies used were mouse anti FLAG
902 (M2 clone) (Millipore Sigma, F3165-1MG), mouse anti EF1α (CBP-KK1 clone) (Millipore
903 Sigma, 05-235), and rabbit anti γ-H2A was a kind gift from Galadriel Hovel-Miner based
904 upon Glover and Horn[78].
905
906 **Flow cytometry:**
907 In 96 well plates, 200,000 parasites were stained with 1:20,000 rabbit anti
908 AnTat1.1 primary antibody[29] (Jay Bangs) for ten minutes at 4C while shaking in PBS +
909 10mg/mL glucose. Parasites were washed once with 100uL PBS + glucose. Then,
910 parasites were stained with Alexa Fluor 647-conjugated goat anti rabbit IgG (H+L),
911 F(ab')2 Fragment (Cell Signaling, 4414S) at 1:1000 at 4C while shaking in PBS + glucose.
912 After washing again with 100uL PBS + glucose, parasites were resuspended in PBS +
913 glucose + 1:20 Propidium Iodide (BD Biosciences, 556463) and analyzed on a Attune Nxt
914 flow cytometer (Invitrogen). Data analysis was performed using FlowJo v10.
915
916 **Analysis and modeling of VSG N-terminal domains:**
917 Full length protein coding sequences from AnTat1.1 and its isolated mosaics were
918 used for structural modeling. Only N-terminal domain sequences were used for protein
919 structural prediction since this region of the VSG is the most well-defined experimentally.
920 Signal peptides are cleaved from the mature VSG during processing, so we used SignalP
921 6.0[79] to predict and remove the Sec/SPI sequence (--organism eukarya, --mode fast)
922 resulting in a FASTA file of mature proteins. To determine the coordinate of the N-terminal
923 domain, we used a python analysis pipeline available at
924 (https://github.com/mugnierlab/find_VSG_Ndomains). The script identifies the
925 boundaries of the VSG N-terminal domain using the HMMscan function under HMMer
926 version 3.1b2[80]. Query sequences are searched against an HMM profile containing 735
927 known N-terminal domain sequences from Cross et al.[2] and N-terminal domains defined
928 by the largest envelope domain coordinate that meets E value threshold (1×10^{-5}, -domE
929 0.00001). The processed FASTA file containing only mature VSG N-terminal domain
930 sequences was used as input for structural prediction of monomers using
931 LocalColabFold[30] function colabfold_batch run using the following arguments: --amber, -
932 -templates, --num_recycle 3. The best ranked output model with the highest average
933 predicted local distance test score (pLDDT), that is the highest confidence model, was
934 used for downstream analyses. Model visualization and alignment were performed using
935 with UCSF ChimeraX version 1.7.1[81], developed by the Resource for Biocomputing,

Visualization, and Informatics at the University of California, San Francisco, with support from National Institutes of Health R01-GM129325 and the Office of Cyber Infrastructure and Computational Biology, National Institute of Allergy and Infectious Diseases.

Acknowledgements

We would like to thank Jay Bangs for generating and sending us primary rabbit anti-AnTat1.1 polyclonal antibody. Thanks to Galadriel Hovel-Miner for the primary rabbit anti-γ-H2A antibody. We appreciate members of the Mugnier lab for their thoughtful review of this manuscript, particularly Carolina Duque and Sneider Gutierrez. We also would like to thank Richard McCulloch for thoughtful feedback about this manuscript. We would like to thank David Mohr and the JHU GCRF Genomics Core for sequencing services. Thanks to Joey Verdi for pHH-HYG-VSG-3-S317A and advice about the generation of transgenic parasites. Data analysis was carried out at the Advanced Research Computing at Hopkins (ARCH) core facility (rockfish.jhu.edu), which is supported by the National Science Foundation (NSF) grant number OAC 1920103. This work was supported by the JHU Catalyst Award. JES, JMCH, AKB, JS, BZ, and MRM were supported by Office of the Director, NIH (DP5OD023065). JES and JS were additionally supported NIH training grant T32GM007 and JES was supported by the National Science Foundation (NSF) Graduate Research Fellowship under grant numbers 1232825 and 1746891. JMCH, AKB, JS and EHA were additionally supported by NIH T32AI007417.

Author Contributions

Conceptualization, J.E.S. and M.R.M.; Methodology, J.E.S., J.M.C.H., A.K.B., A.M., S.D.G., B.Z., and E.H.A.; Software, J.E.S., A.M., J.S., and L.M.; Validation, J.E.S. and K.J.W.; Formal Analysis, J.E.S.; Investigation, J.E.S., K.J.W., E.M.K., J.S., A.K.B., A.M., J.Z., and D.N.M.; Resources, M.R.M.; Data Curation, J.E.S., A.M., and J.S.; Writing – Original Draft, J.E.S. and M.R.M.; Writing – Reviewing & Editing, J.E.S., A.K.B., and M.R.M.; Visualization, J.E.S. and J.S.; Supervision, J.E.S. and M.R.M.; Project Administration, J.E.S.; Funding Acquisition, J.E.S. and M.R.M.

VSG-AMP-seq developed by J.E.S., S.D.G., and B.Z. EATRO1125 Cas9 experiments performed by J.E.S. Lister427 Cas9 and Lister427-Cas9-AnTat1.1 experiments performed by J.E.S. Lister427-Cas9-AnTat1.1 with VSG-228 experiments performed by K.J.W. Molecular cloning performed by J.E.S., K.J.W., E.M.K., and D.N.M. Transgenic parasites obtained by J.E.S., K.J.W., and E.M.K. Western blots performed by J.E.S. and E.M.K. VSG-AMP-seq pipeline written by J.E.S. RNA extractions, DNase treatment, and VSG PCRs for sequencing performed by J.E.S., K.J.W., and A.K.B. VSG-seq performed by J.E.S and A.K.B. VSG-AMP-seq performed by J.E.S. and K.J.W. Mouse infections and all downstream analysis performed by J.E.S. ORF mosaic recombination identification was performed by J.E.S. and A.M. Mosaic parasite clones processed for sequencing by J.E.S., K.J.W., and J.Z. FACS experiments and analysis performed by J.E.S. Modeling of VSGs performed by J.S. and L.M. Lister427 2018 VSG annotation pipeline written by J.E.S. VSG clustering performed by J.E.S., J.S., A.M., J.M.C.H., and E.H.A.

Declaration of Interests

The authors declare no competing interests.

986 **Supplemental Information**
987 Document S1. Figures S1-S5
988 Table1.
989
990 **References**

991 1. Hertz-Fowler, C. *et al.* Telomeric Expression Sites Are Highly Conserved in
992 Trypanosoma brucei. *PLoS ONE* **3**, e3527 (2008).
993 2. Cross, G. A. M., Kim, H.-S. & Wickstead, B. Capturing the variant surface
994 glycoprotein repertoire (the VSGnome) of Trypanosoma brucei Lister 427. *Mol.*
995 *Biochem. Parasitol.* **195**, 59–73 (2014).
996 3. Mugnier, M. R., Cross, G. A. M. & Papavasiliou, F. N. The in vivo dynamics of
997 antigenic variation in *Trypanosoma brucei*. *Science* **347**, 1470–1473 (2015).
998 4. Beaver, A. *et al.* Extravascular spaces are reserviors of antigenic diversity in
999 Trypanosoma bruci infection. *bioRxiv* (2022)
1000 doi:https://doi.org/10.1101/2022.06.27.497797.
1001 5. Hall, J. P. J., Wang, H. & Barry, J. D. Mosaic VSGs and the Scale of Trypanosoma
1002 brucei Antigenic Variation. *PLoS Pathog.* **9**, e1003502 (2013).
1003 6. Roth, C., Bringaud, F., Layden, R. E., Baltz, T. & Eisen, H. Active late-appearing
1004 variable surface antigen genes in Trypanosoma equiperdum are constructed entirely
1005 from pseudogenes. *Proc. Natl. Acad. Sci.* **86**, 9375–9379 (1989).
1006 7. So, J. *et al.* VSGs Expressed during Natural T. b. gambiense Infection Exhibit
1007 Extensive Sequence Divergence and a Subspecies-Specific Bias towards Type B N-
1008 Terminal Domains. *mBio* **13**, e02553-22 (2022).
1009 8. Pays, E. *et al.* Gene conversion as a mechanism for antigenic variation in
1010 Trypanosomes. *Cell* **34**, 371–381 (1983).
1011 9. Baltz, T. *et al.* Exposed epitopes on a Trypanosoma equiperdum variant surface
1012 glycoprotein altered by point mutations. *EMBO J.* **10**, 1653–1659 (1991).
1013 10. Pays, E. *et al.* Trypanosoma brucei: The extent of conversion in antigen genes may
1014 be related to the DNA coding specificity. *Cell* **42**, 821–829 (1985).
1015 11. Pays, E. *et al.* Modifications of a trypanosoma b. brucei antigen gene repertoire by
1016 different DNA recombinational mechanisms. *Cell* **35**, 721–731 (1983).
1017 12. Pays, E. *et al.* At least two transposed sequences are associated in the expression
1018 site of a surface antigen gene in different Trypanosome clones. *Cell* **34**, 359–369
1019 (1983).
1020 13. Kamper, S. M. & Barbet, A. F. Surface epitope variation via mosaic gene formation
1021 is potential key to long-term survival of Trypanosoma brucei. *Mol. Biochem.*
1022 *Parasitol.* **53**, 33–44 (1992).
1023 14. Thon, G., Baltz, T. & Eisen, H. Antigenic diversity by the recombination of
1024 pseudogenes. *Genes Dev.* **3**, 1247–1254 (1989).
1025 15. Lu, Y., Hall, T., Gay, L. S. & Donelson, J. E. Point mutations are associated with a
1026 gene duplication leading to the bloodstream reexpression of a trypanosome
1027 metacyclic VSG. *Cell* **72**, 397–406 (1993).
1028 16. Rice-Ficht, A. C., Chen, K. K. & Donelson, J. E. Point mutations during generation of
1029 expression-linked extra copy of trypanosome surface glycoprotein gene. *Nature* **298**,
1030 676–679 (1982).

1031 17. Lu, Y., Alarcon, C. M., Hall, T., Reddy, L. V. & Donelson, J. E. A strand bias occurs
1032 in point mutations associated with variant surface glycoprotein gene conversion in
1033 Trypanosoma rhodesiense. *Mol. Cell. Biol.* **14**, 3971–3980 (1994).
1034 18. Berriman, M. *et al.* The architecture of variant surface glycoprotein gene expression
1035 sites in Trypanosoma brucei. *Mol. Biochem. Parasitol.* **122**, 131–140 (2002).
1036 19. Boothroyd, C. E. *et al.* A yeast-endonuclease-generated DNA break induces
1037 antigenic switching in Trypanosoma brucei. *Nature* **459**, 278–281 (2009).
1038 20. Glover, L., Alsford, S. & Horn, D. DNA Break Site at Fragile Subtelomeres
1039 Determines Probability and Mechanism of Antigenic Variation in African
1040 Trypanosomes. *PLoS Pathog.* **9**, e1003260 (2013).
1041 21. Kou, R. *et al.* Benefits and Challenges with Applying Unique Molecular Identifiers in
1042 Next Generation Sequencing to Detect Low Frequency Mutations. *PLOS ONE* **11**,
1043 e0146638 (2016).
1044 22. Kanagawa, T. Bias and artifacts in multitemplate polymerase chain reactions (PCR).
1045 *J. Biosci. Bioeng.* **96**, 317–323 (2003).
1046 23. Müller, L. S. M. *et al.* Genome organization and DNA accessibility control antigenic
1047 variation in trypanosomes. *Nature* **563**, 121–125 (2018).
1048 24. Marcello, L. & Barry, J. D. Analysis of the VSG gene silent archive in Trypanosoma
1049 brucei reveals that mosaic gene expression is prominent in antigenic variation and is
1050 favored by archive substructure. *Genome Res.* **17**, 10 (2007).
1051 25. Berriman, M. *et al.* The Genome of the African Trypanosome *Trypanosoma brucei*.
1052 *Science* **309**, 416–422 (2005).
1053 26. Bernards, A. *et al.* Rapid change of the repertoire of variant surface glycoprotein
1054 genes in trypanosomes by gene duplication and deletion. *J. Mol. Biol.* **190**, 1–10
1055 (1986).
1056 27. Aline, R. *et al.* $(TAA)_n$ within sequences flanking several intrachromosomal variant
1057 surface glycoprotein genes in *Trypanosoma brucei*. *Nucleic Acids Res.* **13**, 3161–
1058 3177 (1985).
1059 28. Kitamura, D., Roes, J., Kühn, R. & Rajewsky, K. A B cell-deficient mouse by
1060 targeted disruption of the membrane exon of the immunoglobulin μ chain gene.
1061 *Nature* **350**, 423–426 (1991).
1062 29. Gruszynski, A. E., DeMaster, A., Hooper, N. M. & Bangs, J. D. Surface Coat
1063 Remodeling during Differentiation of Trypanosoma brucei. *J. Biol. Chem.* **278**,
1064 24665–24672 (2003).
1065 30. Mirdita, M. *et al.* ColabFold: making protein folding accessible to all. *Nat. Methods*
1066 **19**, 679–682 (2022).
1067 31. Barnes, R. L. & McCulloch, R. Trypanosoma brucei homologous recombination is
1068 dependent on substrate length and homology, though displays a differential
1069 dependence on mismatch repair as substrate length decreases. *Nucleic Acids Res.*
1070 **35**, 3478–3493 (2007).
1071 32. McCulloch, R. & Barry, J. D. A role for RAD51 and homologous recombination in
1072 Trypanosoma brucei antigenic variation. *Genes Dev.* **13**, 2875–2888 (1999).
1073 33. Conway, C., Proudfoot, C., Burton, P., Barry, J. D. & McCulloch, R. Two pathways of
1074 homologous recombination in *Trypanosoma brucei*. *Mol. Microbiol.* **45**, 1687–1700
1075 (2002).

1076 34. Glover, L., Jun, J. & Horn, D. Microhomology-mediated deletion and gene
1077 conversion in African trypanosomes. *Nucleic Acids Res.* **39**, 1372–1380 (2011).
1078 35. McCulloch, R., Morrison, L. J. & Hall, J. P. J. DNA Recombination Strategies During
1079 Antigenic Variation in the African Trypanosome. *Microbiol. Spectr.* **3**, 3.2.03 (2015).
1080 36. Burton, P., McBride, D. J., Wilkes, J. M., Barry, J. D. & McCulloch, R. Ku
1081 Heterodimer-Independent End Joining in *Trypanosoma brucei* Cell Extracts Relies
1082 upon Sequence Microhomology. *Eukaryot. Cell* **6**, 1773–1781 (2007).
1083 37. Mehnert, A.-K. *et al.* The MRN complex promotes DNA repair by homologous
1084 recombination and restrains antigenic variation in African trypanosomes. *Nucleic*
1085 *Acids Res.* **49**, 1436–1454 (2021).
1086 38. Marin, P. A., Da Silva, M. S., Pavani, R. S., Machado, C. R. & Elias, M. C.
1087 Recruitment kinetics of the homologous recombination pathway in procyclic forms of
1088 Trypanosoma brucei after ionizing radiation treatment. *Sci. Rep.* **8**, 5405 (2018).
1089 39. Wickstead, B., Ersfeld, K. & Gull, K. The Small Chromosomes of *Trypanosoma*
1090 *brucei* Involved in Antigenic Variation Are Constructed Around Repetitive
1091 Palindromes. *Genome Res.* **14**, 1014–1024 (2004).
1092 40. Ersfeld, K. & Gull, K. Partitioning of Large and Minichromosomes in *Trypanosoma*
1093 *brucei*. *Science* **276**, 611–614 (1997).
1094 41. Hovel-Miner, G., Mugnier, M. R., Goldwater, B., Cross, G. A. M. & Papavasiliou, F.
1095 N. A Conserved DNA Repeat Promotes Selection of a Diverse Repertoire of
1096 Trypanosoma brucei Surface Antigens from the Genomic Archive. *PLOS Genet.* **12**,
1097 e1005994 (2016).
1098 42. Đaković, S. *et al.* A structural classification of the variant surface glycoproteins of the
1099 African trypanosome. *PLoS Negl. Trop. Dis.* **17**, e0011621 (2023).
1100 43. Sheader, K. *et al.* Variant surface glycoprotein RNA interference triggers a
1101 precytokinesis cell cycle arrest in African trypanosomes. *Proc. Natl. Acad. Sci.* **102**,
1102 8716–8721 (2005).
1103 44. Tenaglia, A. H. *et al.* Antibodies to protozoan variable surface antigens induce
1104 antigenic variation. *bioRxiv* (2022) doi:10.1101/2022.06.21.497077.
1105 45. Nenarokova, A. *et al.* Causes and Effects of Loss of Classical Nonhomologous End
1106 Joining Pathway in Parasitic Eukaryotes. *mBio* **10**, e01541-19 (2019).
1107 46. Zhang, X. *et al.* Rapid antigen diversification through mitotic recombination in the
1108 human malaria parasite Plasmodium falciparum. *PLOS Biol.* **17**, e3000271 (2019).
1109 47. Bopp, S. E. R. *et al.* Mitotic Evolution of Plasmodium falciparum Shows a Stable
1110 Core Genome but Recombination in Antigen Families. *PLoS Genet.* **9**, e1003293
1111 (2013).
1112 48. Claessens, A. *et al.* Generation of Antigenic Diversity in Plasmodium falciparum by
1113 Structured Rearrangement of Var Genes During Mitosis. *PLoS Genet.* **10**, e1004812
1114 (2014).
1115 49. Bull, P. C. *et al. Plasmodium falciparum* antigenic variation. Mapping mosaic *var*
1116 gene sequences onto a network of shared, highly polymorphic sequence blocks.
1117 *Mol. Microbiol.* **68**, 1519–1534 (2008).
1118 50. Yang, Y. & Adam, R. D. A group of Giardia lamblia variant-specific surface protein
1119 (VP) genes with nearly identical 5 ' regions. *Mol. Biochem. Parasitol.* **75**, 69–74
1120 (1995).

1121 51. Adam, R. D. *et al.* The Giardia lamblia vsp gene repertoire: characteristics, genomic
1122 organization, and evolution. *BMC Genomics* **11**, 424 (2010).
1123 52. Del Portillo, H. A. *et al.* A superfamily of variant genes encoded in the subtelomeric
1124 region of Plasmodium vivax. *Nature* **410**, 839–842 (2001).
1125 53. Hall, N. *et al.* A Comprehensive Survey of the *Plasmodium* Life Cycle by Genomic,
1126 Transcriptomic, and Proteomic Analyses. *Science* **307**, 82–86 (2005).
1127 54. Del Portillo, H. A., Lanzer, M., Rodriguez-Malaga, S., Zavala, F. & Fernandez-
1128 Becerra, C. Variant genes and the spleen in Plasmodium vivax malaria. *Int. J.*
1129 *Parasitol.* **34**, 1547–1554 (2004).
1130 55. Schimmel, J., van Schendel, R., den Dunnen, J. T. & Tijsterman, M. Templated
1131 Insertions: A Smoking Gun for Polymerase Theta-Mediated End Joining. *Trends*
1132 *Genet.* **35**, 632–644 (2019).
1133 56. Williams, D. L. *et al.* May the Odds Be Ever in Your Favor: Non-deterministic
1134 Mechanisms Diversifying Cell Surface Molecule Expression. *Front. Cell Dev. Biol.* **9**,
1135 720798 (2022).
1136 57. Zozulya, S., Echeverri, F. & Nguyen, T. The human olfactory receptor repertoire.
1137 *Genome Biol.* **2**, research0018.1 (2001).
1138 58. Lai, P. C. *et al.* An olfactory receptor pseudogene whose function emerged in
1139 humans: a case study in the evolution of structure–function in GPCRs. *J. Struct.*
1140 *Funct. Genomics* **9**, 29–40 (2008).
1141 59. Niimura, Y. & Nei, M. Evolution of olfactory receptor genes in the human genome.
1142 *Proc. Natl. Acad. Sci.* **100**, 12235–12240 (2003).
1143 60. Newman, T. & Trask, B. J. Complex Evolution of 7E Olfactory Receptor Genes in
1144 Segmental Duplications. *Genome Res.* **13**, 781–793 (2003).
1145 61. Noonan, J. P., Grimwood, J., Schmutz, J., Dickson, M. & Myers, R. M. Gene
1146 Conversion and the Evolution of Protocadherin Gene Cluster Diversity. *Genome*
1147 *Res.* **14**, 354–366 (2004).
1148 62. Wirtz, E., Leal, S., Ochatt, C. & Cross, GeorgeA. M. A tightly regulated inducible
1149 expression system for conditional gene knock-outs and dominant-negative genetics
1150 in Trypanosoma brucei. *Mol. Biochem. Parasitol.* **99**, 89–101 (1999).
1151 63. Isothermal Reaction (Gibson Assembly) Master Mix. *Cold Spring Harb. Protoc.*
1152 **2017**, pdb.rec090019 (2017).
1153 64. Rico, E., Jeacock, L., Kovářová, J. & Horn, D. Inducible high-efficiency CRISPR-
1154 Cas9-targeted gene editing and precision base editing in African trypanosomes. *Sci.*
1155 *Rep.* **8**, 7960 (2018).
1156 65. Gkeka, A. *et al.* Immunodominant surface epitopes power immune evasion in the
1157 African trypanosome. *Cell Rep.* **42**, 112262 (2023).
1158 66. Shaw, S., Knüsel, S., Hoenner, S. & Roditi, I. A transient CRISPR/Cas9 expression
1159 system for genome editing in Trypanosoma brucei. *BMC Res. Notes* **13**, 268 (2020).
1160 67. Zheng, Z. *et al.* Anchored multiplex PCR for targeted next-generation sequencing.
1161 *Nat. Med.* **20**, 1479–1484 (2014).
1162 68. Tsai, S. Q. *et al.* GUIDE-seq enables genome-wide profiling of off-target cleavage by
1163 CRISPR-Cas nucleases. *Nat. Biotechnol.* **33**, 187–197 (2015).
1164 69. Martin, M. Cutadapt removes adapter sequences from high-throughput sequencing
1165 reads. *EMB.journal* **17**,.

70. Fu, L., Niu, B., Zhu, Z., Wu, S. & Li, W. CD-HIT: accelerated for clustering the next-generation sequencing data. *Bioinformatics* **28**, 3150–3152 (2012).
71. Li, W. & Godzik, A. Cd-hit: a fast program for clustering and comparing large sets of protein or nucleotide sequences. *Bioinformatics* **22**, 1658–1659 (2006).
72. Langmead, B., Trapnell, C., Pop, M. & Salzberg, S. L. Ultrafast and memory-efficient alignment of short DNA sequences to the human genome. *Genome Biol.* **10**, R25 (2009).
73. Amos, B. *et al.* VEuPathDB: the eukaryotic pathogen, vector and host bioinformatics resource center. *Nucleic Acids Res.* **50**, D898–D911 (2022).
74. Csardi, G. & Nepusz, T. The igraph software package for complex network research. *InterJournal* Complex Systems **1695**, (2006). https://igraph.org.
75. Csárdi, G. *et al.* igraph for R: R interface of the igraph library for graph theory and network analysis. Zenodo https://doi.org/10.5281/ZENODO.7682609 (2024).
76. Edgar, R. C. Search and clustering orders of magnitude faster than BLAST. *Bioinformatics* **26**, 2460–2461 (2010).
77. Schindelin, J. *et al.* Fiji: an open-source platform for biological-image analysis. *Nat. Methods* **9**, 676–682 (2012).
78. Glover, L. & Horn, D. Trypanosomal histone γH2A and the DNA damage response. *Mol. Biochem. Parasitol.* **183**, 78–83 (2012).
79. Teufel, F. *et al.* SignalP 6.0 predicts all five types of signal peptides using protein language models. *Nat. Biotechnol.* **40**, 1023–1025 (2022).
80. Eddy, S. R. Accelerated Profile HMM Searches. *PLoS Comput. Biol.* **7**, e1002195 (2011).
81. Meng, E. C. *et al.* UCSF CHIMERAX : Tools for structure building and analysis. *Protein Sci.* **32**, e4792 (2023).

1193 **Supplemental figures**

1194

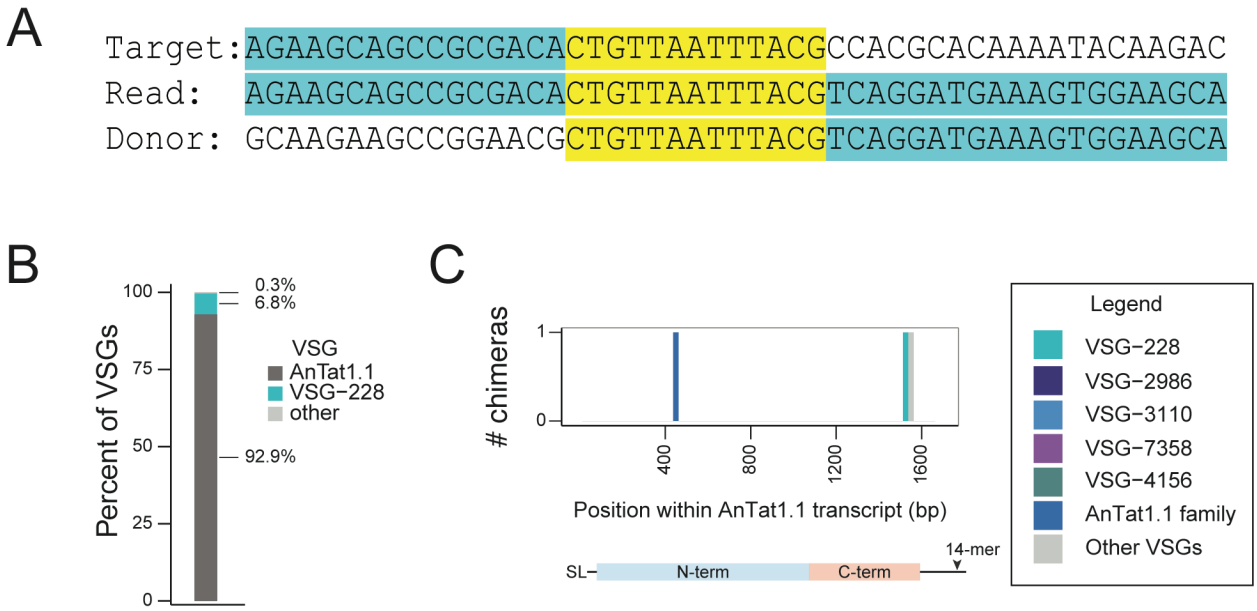

Supplemental Figure 1. Mosaic Recombination Site & VSG-AMP-seq Validation
A) A schematic of a recombination site. The region in yellow is the putative recombination site, shared by all 3 sequences. B) A stacked bar graph quantifying the mix of Lister427 parasites engineered to express either AnTat1.1 or VSG-228 as determined by VSG-seq. These VSGs are naturally absent from Lister427 parasites and therefore chimeric reads containing sequence from both VSGs must have arisen from error. C) A histogram showing the midpoint of chimeric recombination events misidentified as a mosaic VSGs by VSG-AMP-seq from the mixed parasite sample in Supplemental Figure 1B.

1195

1196

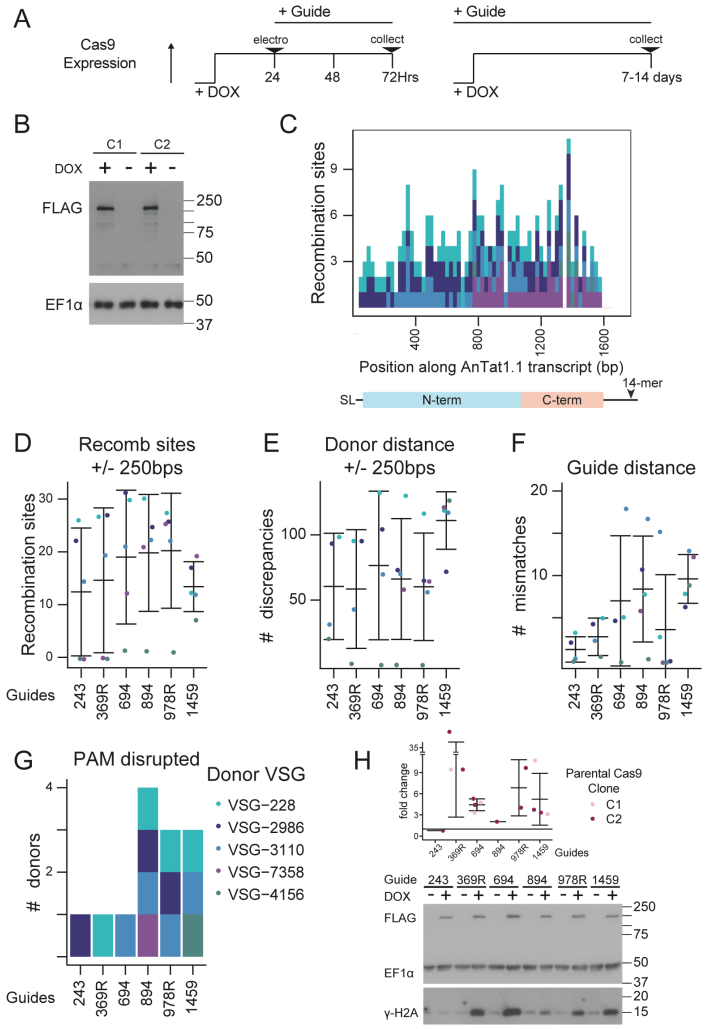

Supplemental Figure 2. Cas9 system and sgRNA design and analysis

A) A schematic of the Cas9 induction experiment. Transient electroporation shown on the left while constitutive guide expression to isolate mosaic clones shown at right. B) An immunoblot showing FLAG-tagged Cas9 induction 24 hours following doxycycline treatment (DOX). DMSO was used as a vehicle control. EF1α was used as a loading control. C) A histogram showing the midpoint of all possible recombination sites 5bps or longer between AnTat1.1 and its family members. D) Quantification of the number of recombination sites within 250bps up or downstream of the cut site for each donor VSG. Mean ± s.d. E) Quantification of the Levenshtein distance between AnTat1.1 and family members. This includes mismatches, insertions and deletions. Mean ± s.d. F) Quantification of the number of mismatches at the guide binding site between AnTat1.1 and family members. Mean ± s.d. G) Histogram of which donor VSGs can disrupt the PAM when used to repair AnTat1.1. H) Quantification of the induction of DNA damage following guide induction as measured by a proxy of DNA damage, γ-H2A phosphorylation, following 24 hours of induction. γ-H2A induction was normalized to EF1α loading and fold change of staining intensity was determined between doxycycline-induced and uninduced samples. DMSO was used as a vehicle control. Mean ± s.d. Below, a representative immunoblot of FLAG, EF1α, and γ-H2A from doxycycline induced clones and uninduced controls is shown. Multiple independently-generated clones were induced. SL = 5′ splice leader sequence, 14-mer = 3′ sequence conserved in all VSG transcripts

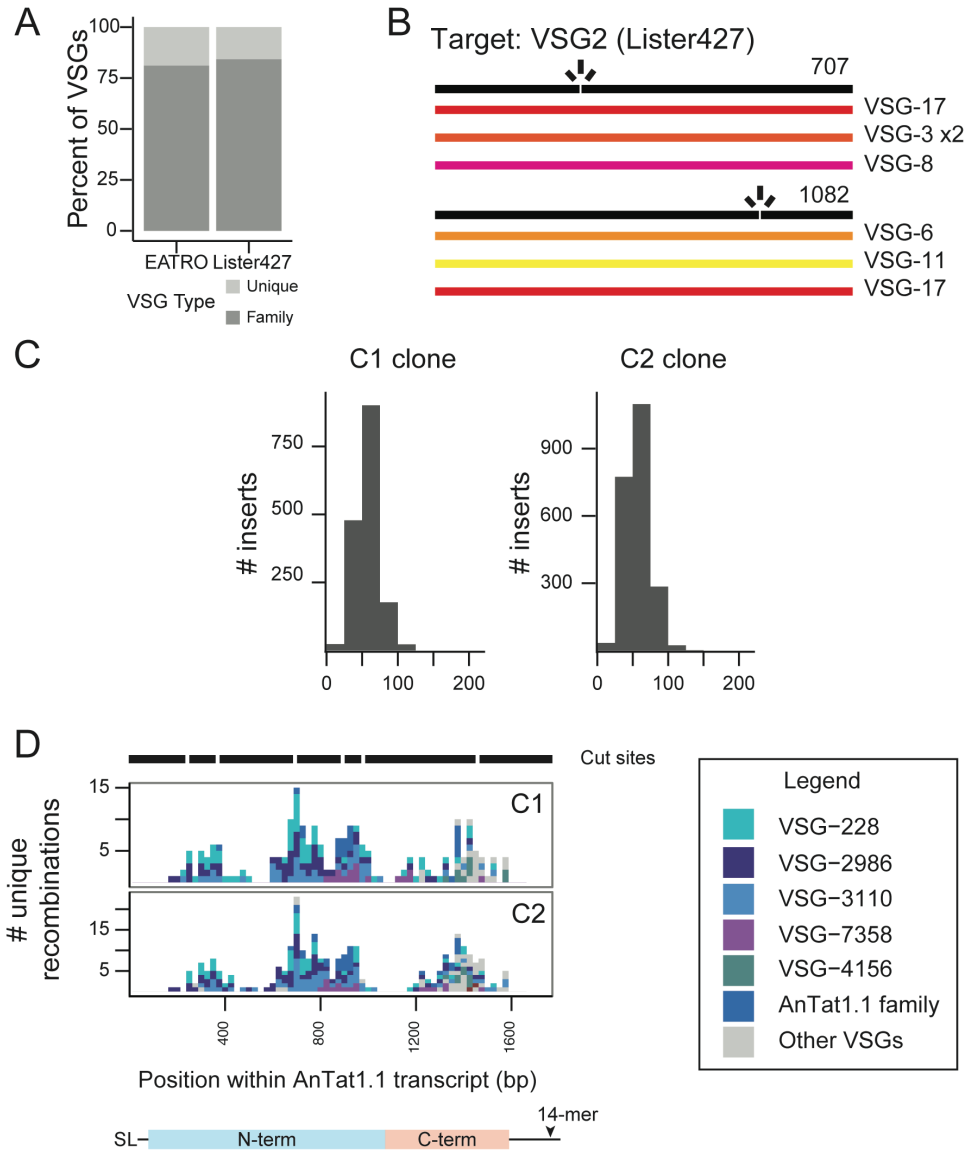

Supplemental Figure 3. DNA breaks result in switchers if a homologous donor is not present
A) Quantification of the types of VSGs within the VSGnomes from EATRO1125 and Lister427 Parasites using the UCLUST greedy clustering algorithm. The Lister427 VSGnome has 4 VSGs which are perfectly duplicated without other family members. B) A schematic showing identified switchers following a Cas9-induced double strand break within VSG-2 at locations 707 and 1082. C) Histograms of donor VSG insertion lengths identified in all mosaic VSG reads from Figure 2A). The insert length only includes newly inserted sequence and does not include recombination sites. Clone C1 and C2 sequenced via VSG-AMP-seq are shown separately. The limit of detection for an insertion is approximately 200 bp. D) A histogram with a summary of the unique recombination sites found within guide-induced break for each clone. Cut sites are indicated above the histograms as gaps within the black line. The midpoint of the perfect homology between AnTat1.1 and the donor VSG at the recombination site is plotted. If a mosaic sequence matched >1 potential donor VSG, the average recombination position was plotted. The legend for the donor VSG colors is to the right. SL = 5′ splice leader sequence, 14-mer = 3′ sequence conserved in all VSG transcripts

1199

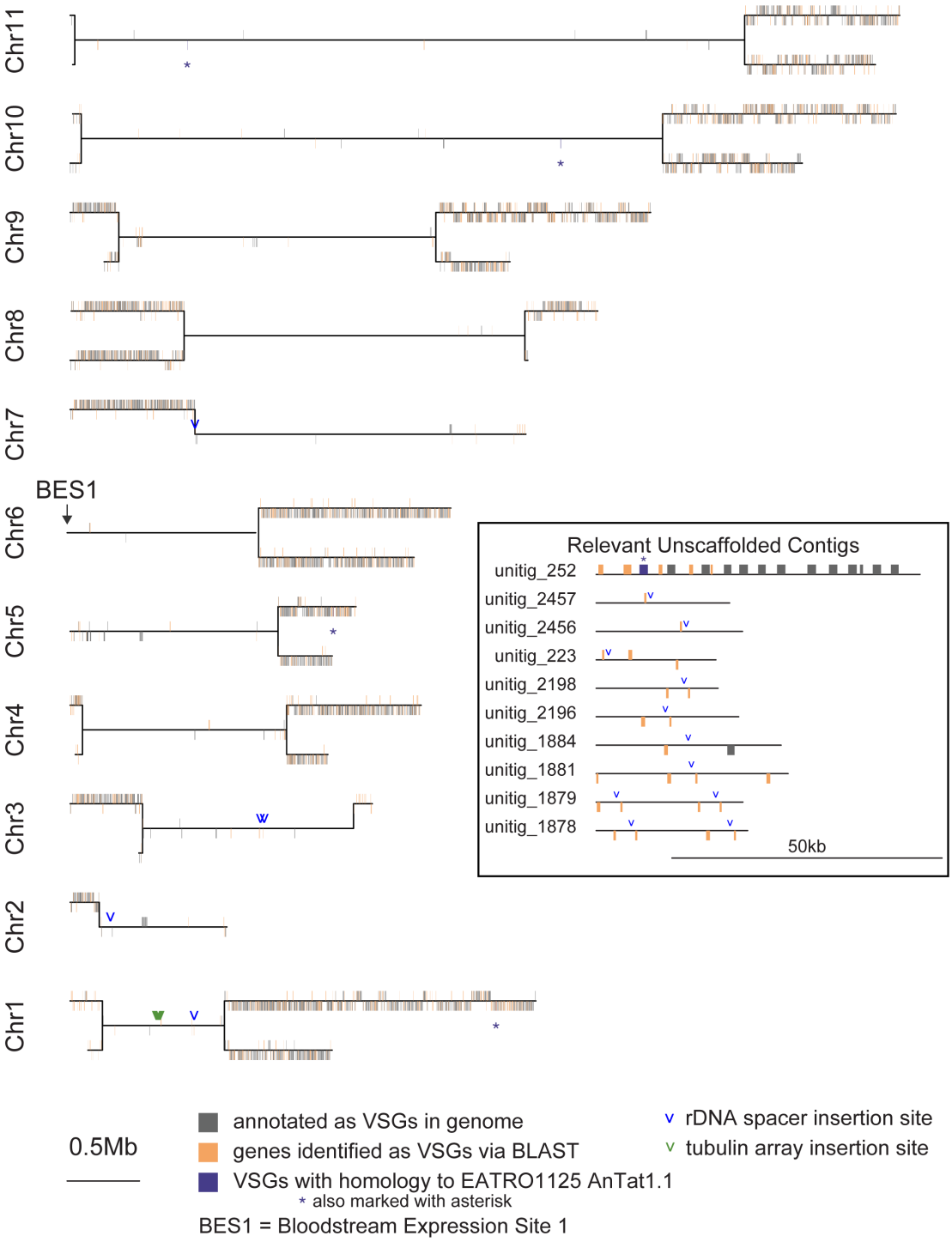

Supplemental Figure 4. The Lister427 VSG annotated genome
The megabase chromosomes from Müller et al.[23] VSGs annotated in the genome are plotted in gray. Unknown genes identified as VSGs via BLAST are plotted in yellow. Details of how these VSGs were identified are detailed in Methods. AnTat1.1 homologous family members are colored purple and marked with an asterisk. Insertion sites for the VSG-228 are denoted by arrows at the insertion location. Inset are the unitigs which are unscaffolded and harbor a copy of the AnTat1.1 family member or a potential insertion site. Bloodstream Expression Site 1 (BES1) is on the 5' end of chromosome 6 and is marked by an arrow.

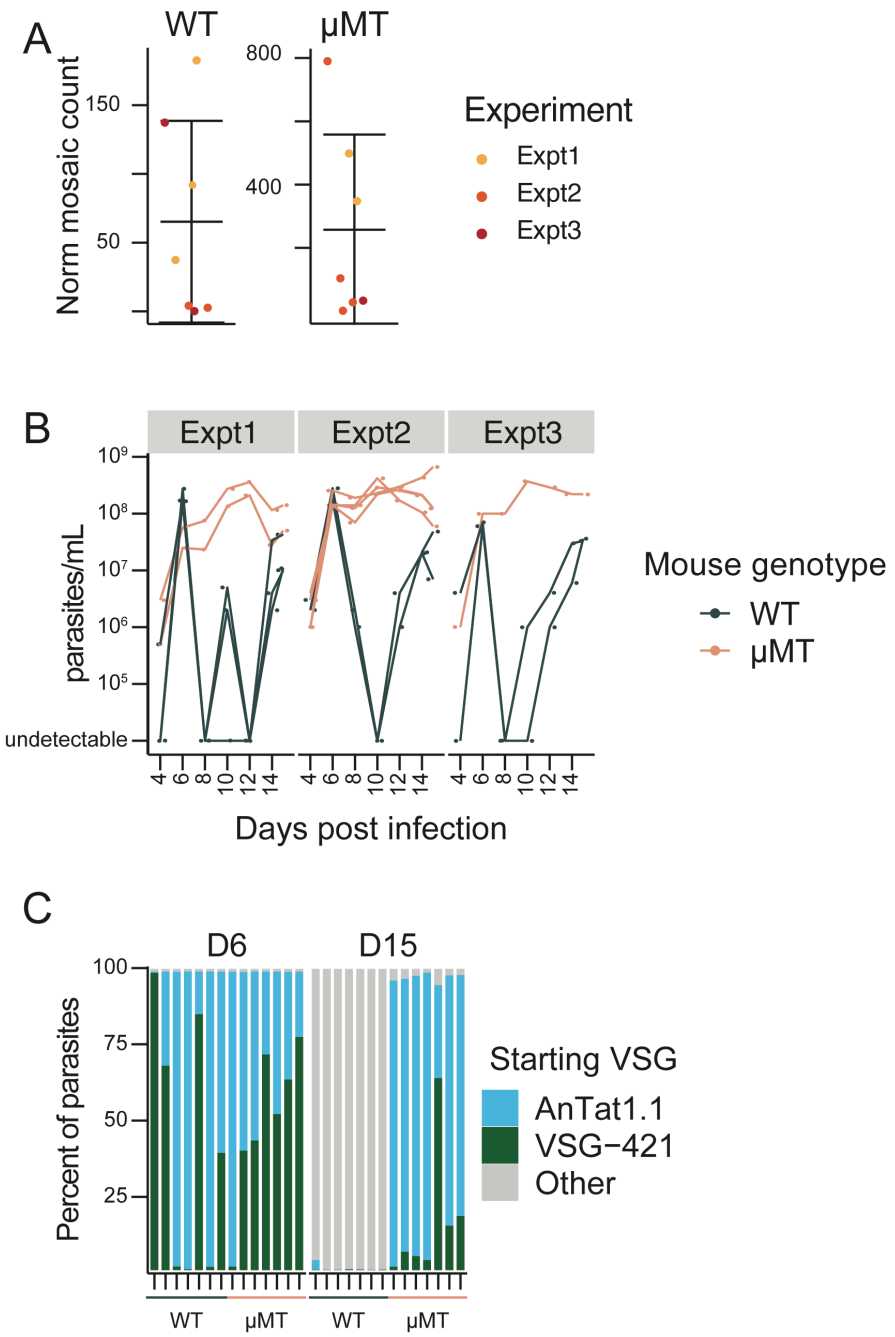

Supplemental Figure 5. Mouse infection extended data
A) Quantification of the number of recombination events detected per mouse. Each mouse was normalized to the number of total consolidated, aligned, and unanchored reads compared to the consolidated, aligned, unanchored read count for one mouse to control for sequencing depth. This was performed separately for each genotype. Mean ± s.d. B) A time course of the parasitemia for the mouse infections. Blood was harvested every two days. C) Quantification of the percent of parasites expressing the starting VSG at D6 and D15 post-infection as quantified by VSG-seq.

1202 Table 1 Guide and VSG-AMP-seq primers

Guide Primers		
Primer Name	Sequence	
AnTat1.1_243	GAAATTAATACGACTCACTATAGGATTCAAAAACGGCCAAACGCCGTTTTAGAGCTAGAAATAGC	
AnTat1.1_369R	GAAATTAATACGACTCACTATAGGGGCGTAAATTAACAGTGTCGGTTTTAGAGCTAGAAATAGC	
AnTat1.1_694	GAAATTAATACGACTCACTATAGGAGTACAGACCCAGAAGCCAGGTTTTAGAGCTAGAAATAGC	
AnTat1.1_894	GAAATTAATACGACTCACTATAGGACGCCGGTGTCGCAGCTAAACGTTTTAGAGCTAGAAATAGC	
AnTat1.1_978R	GAAATTAATACGACTCACTATAGGGTCGTTGGCTGCTTGGAGTTGTTTTAGAGCTAGAAATAGC	
AnTat1.1_1459	GAAATTAATACGACTCACTATAGGACCAATCCAGAAAAGTGCAAGTTTTAGAGCTAGAAATAGC	
G00	AAAAGCACCGACTCGGTGCCACTTTTTCAAGTTGATAACGGACTAGCCTTATTTTAACTTGCTATTTCTAGCTCTAAAAC	
Annealed Guides for T7-sgRNA insertion		
Fragment Name	FWD	REV
AnTat1.1_243	AGGGATTCAAAAACGGCCAAACGCC	AAACGGCGTTTGGCCGTTTTTGAAT
AnTat1.1_369R	AGGGGGCGTAAATTAACAGTGTCG	AAACCGACACTGTTAATTTACGCC
AnTat1.1_694	AGGGAGTACAGACCCAGAAGCCAG	AAACCTGGCTTCTGGGTCTGTACT
AnTat1.1_894	AGGGACGCCGGTGTCGCAGCTAAAC	AAACGTTTAGCTGCGACACCGGCGT
AnTat1.1_978R	AGGGGTCGTTGGCTGCTTGGAGTT	AAACAACTCCAAGCAGCCAACGAC
AnTat1.1_1459	AGGGACCAATCCAGAAAAGTGCAA	AAACTTGCACTTTTCTGGATTGGT
VSG-2_707	AGGGACCAACGGCCTCGGCAAAAG	AAACCTTTTGCCGAGGCCGTTGGT
VSG-2_1082	AGGGCCAGTGGCGCAAAACCTGGT	AAACACCAGGTTTTGCGCCACTGG
DNase Verification Primers		
Primer Name	FWD	REV
HSP-70 (Tb927.11.11330)	AGAACACTATCAATGACCCCAAC	CCATGCCCTGGTACATCT
Hyg	ACAGCGGTCATTGACTGGAG	ATTTGTGTACGCCCGACAGT
VSG-AMP-seq Primers		
Primer Name	Sequence	
All-VSG-3'UTR	GTGTTAAAATATATC	

Y-adapter[%]	[Phos]GATCGGAAGAGC*C*A
A01[^]	AATGATACGGCGACCACCGAGATCTACACTAGATCGC(N:252 52525)(N)(N)(N)(N)(N)(N)(N)(N)(N)(N)(N)(N)(N)(N)(N)(N)(N)(N)(N)(N)(N)(N)ACACTCTTTCCCTACACGACGCTCTTCCGA TC*T
A03[^]	AATGATACGGCGACCACCGAGATCTACACTATCCTCT(N:252 52525)(N)(N)(N)(N)(N)(N)(N)(N)(N)(N)(N)(N)(N)(N)(N)(N)(N)(N)(N)(N)(N)(N)ACACTCTTTCCCTACACGACGCTCTTCCGA TC*T
A04[^]	AATGATACGGCGACCACCGAGATCTACACAGAGTAGA(N:252 52525)(N)(N)(N)(N)(N)(N)(N)(N)(N)(N)(N)(N)(N)(N)(N)(N)(N)(N)(N)(N)(N)(N)ACACTCTTTCCCTACACGACGCTCTTCCGA TC*T
A05[^]	AATGATACGGCGACCACCGAGATCTACACGTAAGGAG(N:252 52525)(N)(N)(N)(N)(N)(N)(N)(N)(N)(N)(N)(N)(N)(N)(N)(N)(N)(N)(N)(N)(N)(N)ACACTCTTTCCCTACACGACGCTCTTCCGA TC*T
A06[^]	AATGATACGGCGACCACCGAGATCTACACACTGCATA(N:252 52525)(N)(N)(N)(N)(N)(N)(N)(N)(N)(N)(N)(N)(N)(N)(N)(N)(N)(N)(N)(N)(N)(N)ACACTCTTTCCCTACACGACGCTCTTCCGA TC*T
A07[^]	AATGATACGGCGACCACCGAGATCTACACAAGGAGTA(N:252 52525)(N)(N)(N)(N)(N)(N)(N)(N)(N)(N)(N)(N)(N)(N)(N)(N)(N)(N)(N)(N)(N)(N)ACACTCTTTCCCTACACGACGCTCTTCCGA TC*T
A08[^]	AATGATACGGCGACCACCGAGATCTACACCTAAGCCT(N:252 52525)(N)(N)(N)(N)(N)(N)(N)(N)(N)(N)(N)(N)(N)(N)(N)(N)(N)(N)(N)(N)(N)(N)ACACTCTTTCCCTACACGACGCTCTTCCGA TC*T
A09[^]	AATGATACGGCGACCACCGAGATCTACACGACATTGT(N:252 52525)(N)(N)(N)(N)(N)(N)(N)(N)(N)(N)(N)(N)(N)(N)(N)(N)(N)(N)(N)(N)(N)(N)ACACTCTTTCCCTACACGACGCTCTTCCGA TC*T
A10[^]	AATGATACGGCGACCACCGAGATCTACACACTGATGG(N:252 52525)(N)(N)(N)(N)(N)(N)(N)(N)(N)(N)(N)(N)(N)(N)(N)(N)(N)(N)(N)(N)(N)(N)ACACTCTTTCCCTACACGACGCTCTTCCGA TC*T
P5_2	AATGATACGGCGACCACCGAGATCTACAC
P701	CAAGCAGAAGACGGCATACGAGATTCGCCTTAGTGACTGGA GTCCTCTCTATGGGCAGTCGGTGA
P703	CAAGCAGAAGACGGCATACGAGATTTCTGCCTGTGACTGGA GTCCTCTCTATGGGCAGTCGGTGA
P704	CAAGCAGAAGACGGCATACGAGATGCTCAGGAGTGACTGGA GTCCTCTCTATGGGCAGTCGGTGA
P705	CAAGCAGAAGACGGCATACGAGATAGGAGTCCGTGACTGGA GTCCTCTCTATGGGCAGTCGGTGA

P706	CAAGCAGAAGACGGCATACGAGATCATGCCTAGTGACTGGAGTCCTCTCTATGGGCAGTCGGTGA
P707	CAAGCAGAAGACGGCATACGAGATGTAGAGAGGTGACTGGAGTCCTCTCTATGGGCAGTCGGTGA
P708	CAAGCAGAAGACGGCATACGAGATCCTCTCTGGTGACTGGAGTCCTCTCTATGGGCAGTCGGTGA
P709	CAAGCAGAAGACGGCATACGAGATATCACGGTGTGACTGGAGTCCTCTCTATGGGCAGTCGGTGA
P710	CAAGCAGAAGACGGCATACGAGATCGATGTGCGTGACTGGAGTCCTCTCTATGGGCAGTCGGTGA
AnTat1.1_1F[&]	CCTCTCTATGGGCAGTCGGTGAT$(N)_{0-7}$CGCAAACACTACAACGAGCC
AnTat1.1_2F[&]	CCTCTCTATGGGCAGTCGGTGAT$(N)_{0-7}$CAGAATGCGACACGGAAAGC
AnTat1.1_3F[&]	CCTCTCTATGGGCAGTCGGTGAT$(N)_{0-7}$ACGCAGGCGGCTTCAAAACA
AnTat1.1_4F[&]	CCTCTCTATGGGCAGTCGGTGAT$(N)_{0-7}$AACAGCCGCAGCAACCAAAC
AnTat1.1_0R[&]	CCTCTCTATGGGCAGTCGGTGAT$(N)_{0-7}$GGCCACAAATGCGGCAGAAAC
AnTat1.1_1R[&]	CCTCTCTATGGGCAGTCGGTGAT$(N)_{0-7}$GCCATAAGCTGCGGTTTCGT
AnTat1.1_2R[&]	CCTCTCTATGGGCAGTCGGTGAT$(N)_{0-7}$GTTGTGTATGGTTAGCAGGC
AnTat1.1_3R[&]	CCTCTCTATGGGCAGTCGGTGAT$(N)_{0-7}$CTTGTATTTTGTGCGTGGCG
Index1[%]	ATCACCGACTGCCCATAGAGAGGACTCCAGTCAC
Read2[%]	GTGACTGGAGTCCTCTCTATGGGCAGTCGGTGAT
Miscellaneous Additional Primers	
Name	Sequence
SL-FWD	ACAGTTTCTGTACTATATTG
SP6-14mer-REV	GATTTAGGTGACACTATAGTGTTAAAATATATC
AnTat1.1 Sanger Sequencing Primer	AGAGAATACTAAGCTAGTTGGC
Pan AnTat1.1family FWD	ACTACACCCACAACAAGCTCTA

[a] * = indicates a phosphorothioate bond modification
[b] [Phos] = 5' phosphorylation
[c] ^ = hand mixing
[d] & = machine mixing
[e] % = HPLC purification